Fire Distinguishers: Refined interpretations of polycyclic aromatic hydrocarbons for paleo-applications

Allison T Karp[1]*, Alex I Holman[2], Peter Hopper[2], Kliti Grice[2], Katherine H Freeman[1]

[1]Department of Geosciences, The Pennsylvania State University, University Park, PA 16802, USA (*amk6331@psu.edu)
[2]WA Organic & Isotope Geochemistry Centre, The Institute for Geoscience Research, School of Earth and Planetary Sciences, Curtin University, Bentley, WA 6102, Australia

Keywords: Polycyclic aromatic hydrocarbons (PAHs); compound-specific $\delta^{13}C$; Paleofire; experimental biomass burning

Target Journal: Geochimica et Cosmochimica Acta

Abstract
Polycyclic aromatic hydrocarbons (PAHs), produced *via* incomplete combustion of organics, convey signatures of vegetation burned in the geologic past. New and published burn experiments reveal how the quantity, distributions, and isotopic abundances of fire-derived PAHs were influenced by fuel types, burn conditions, and also phase. PAH concentrations were higher in burn residues from moderate burn temperatures (400-500 ºC), and significantly lower in residues from cooler (<300ºC) or hotter (>600ºC) conditions, especially when oxygen was limited. PAH forms tended to be smaller in smoke samples and larger in residues, consistent with molecular physical and chemical properties. Plant functional types were distinguished by relative amounts of retene and dimethyl phenanthrene isomers. Isotopically distinct photosynthetic pathways of the burned material were reflected in the $\delta^{13}C$ values of PAHs, which faithfully captured biomass signatures as well as the ~12‰ offset between C_3 and C_4 plant types. PAH size, alkylation, and isotope characteristics can differentiate combusted plant types and distinguish between air-borne and sedimentary transport mechanisms. New proxy approaches using PAH amounts, distributions, and isotope signatures can aid and refine interpretations of paleofire ecology in the geologic record.

1. Introduction

Human activities are changing wildfire patterns both regionally and globally (Bowman et al., 2009; Archibald et al., 2017). Earth history offers many potential insights into how wildfire dynamics responded to large climate perturbations in the past and their consequences for the carbon cycle (Daniau et al., 2012; Denis et al., 2017). Rising global temperatures and pCO_2 are fast approaching levels not experienced in the last 30 Myr (Burke et al., 2018). As a result, reconstructions of paleo-fire regimes during the Holocene, Pliocene, and Eocene will continue to grow in importance for predicting future changes in wildfires (Daniau and Brücher, 2016; Burke et al., 2018).

The main variables of interest when reconstructing paleofire are changes in fire occurrence, intensity, area and vegetation community burned. Common proxies for reconstructing ancient fire include abundances of microscopic and macroscopic charcoal and bulk black carbon (Conedera et al., 2009; Thevenon et al., 2010). The reflectance, size, shape, and isotopic composition of charcoal preserve information about fuel source, burn severity, and burn area (Umbanhowar and McGrath, 1998; Duffin et al., 2008; Leys et al., 2017). However, charcoal production and preservation tends to bias towards woody fuels, high temperature burns, and fires proximal to sedimentary records (Umbanhowar and McGrath, 1998; Conedera et al., 2009; Hudspith and Belcher, 2017; Doerr et al., 2018). Molecular proxies for fire complement these bulk parameters, as they have different biases, preservation potential and transport pathways, and preserve additional information in their chemical structures, distributions, and isotopic compositions (Denis et al., 2012; Schneider et al., 2013; Kirchgeorg et al., 2014).

Polycyclic aromatic hydrocarbons (PAHs) can result from incomplete combustion of biomass and fossil fuels (Richter and Howard, 2000; Marynowski and Simoneit, 2009) and are increasingly used as a proxy for vegetation burning in sedimentary records (Denis et al., 2017; Miller et al., 2017; Argiriadis et al., 2018; Callegaro et al., 2018; Karp et al., 2018; Vachula et al.,

2019). Changes in PAH concentrations in geologic archives are commonly interpreted to reflect changes in fire occurrence *via* a combination of changes in fire frequency and intensity (Denis et al., 2012). Biomass burned, high temperatures and low O_2 content have all been linked to higher quantities of PAHs generated during biomass combustion (McGrath et al., 2003; Lu et al., 2009; Kappenberg et al., 2019). Additionally, many paleofire studies interpret changes in PAH size distribution as changes in fire intensity based mainly on the observation that aromaticity in bulk burn products increases with temperature (McGrath et al., 2003; McBeath et al., 2011; Denis et al., 2012). However, many of these interpretations are based on observations from a limited set of burn conditions, and there are strong indications that PAHs behave differently than other pyrogenic parameters in both experimental and environmental settings (Wiedemeier et al., 2015b; Wiedemeier et al., 2015a; Hanke et al., 2016; Santín et al., 2017). Comparisons of PAHs produced under a wide variety of observational and experimental conditions will constrain the relative influence of temperature, O_2 content, burn phase partitioning and fuel source to strengthen interpretations of PAH characteristics.

The fate of PAHs in the environment are linked to their physiochemical properties. PAH molecular size and shape determine their aqueous solubility (C_w^{sat}), affinity for organics (K_{ow}) and volatility (V_p) (Miller et al., 1985; Mackay, 1998; Lima et al., 2005). Smaller compounds have higher vapor pressures and are preferentially emitted with the gaseous phase during biomass combustion (Mackay, 1998; Lima et al., 2005). Larger compounds have lower aqueous solubility and tend to partition more strongly into organic coatings and particles (Mackay, 1998; Lima et al., 2005). In addition, low aqueous solubility hinders biodegradation of PAHs with four or more rings (Mackay, 1998; Lima et al., 2005). Differential partitioning of PAHs between burn phases may impact their preservation, transport, and ultimate fate in soils and sediments. While many studies have examined PAH partitioning between vapor and particulate burn phases in a plume

(e.g., Jenkins et al., 1996; Lima et al., 2005; Shen et al., 2011), few have compared PAH distributions between char residues and smoke aerosol burn phases (Kappenberg et al., 2019).

Modern environmental studies of PAH characteristics tend to focus on differentiating anthropogenic pollutant sources (i.e., residential wood combustion, fossil fuel combustion, and petroleum; (Yunker et al., 2002; Lima et al., 2005; Stogiannidis and Laane, 2015). Parent PAHs (structures without any alkyl-substitutions) are preferentially produced under fast, high-temperature combustion conditions, while structures with one or more alkyl-substitutions are preferentially produced under slow, low-temperature thermogenic reactions (Blumer and Youngblood, 1975; Budzinski et al., 1995). Thus, the relative amounts of alkylated PAHs provide fingerprints of fire-derived *vs*. fossil fuel derived sources (Yunker et al., 2002; Stogiannidis and Laane, 2015; Denis, 2016; Rocha and Palma, 2019). However, there are still uncertainties in how these distributions vary within a set of pyrogenic samples (e.g., Keiluweit et al., 2012).

Wildfire-derived PAHs may preserve additional information about the type of plant community that burned. Previous work has suggested certain alkylated PAH structures and carbon isotopes of PAHs can distinguish between different plant types (Grice et al., 2009; Nabbefeld et al., 2010; Holman and Grice, 2018). Several parameters, such as dimethyl phenanthrene (DMP) ratios, are used as proxies for changes in burned plant community (Yunker et al., 2002; Kappenberg et al., 2019). However, plant-specific PAH distributions and carbon isotopes have been measured far less often than other plant biomarkers (i.e., leaf waxes, terpenoids; Diefendorf and Freimuth, 2017; Nakamura, 2019). The lack of PAH measurements on modern burned plants make it challenging to use these tools to quantitatively reconstruct changes in burned plant communities.

The aim of this study was to improve the use of PAHs in studies of paleofire based on a better understanding of their quantities, distributions, and isotope signatures from controlled burn experiments. We evaluated different fuel, burn conditions and phase to learn which of these

75 factors: 1) might bias PAH quantity as a proxy for fire occurrence 2) can be distinguished by
76 characteristic PAH distributions, and 3) potentially limit the fidelity of carbon isotope signatures
77 for fuels representing different plant groups.
78 We examined relationships between burn conditions and the concentrations, distributions,
79 and carbon isotope values of PAHs from 10 burn experiments on seven different plant taxa. PAH
80 data generated from these experiments were combined with data from six published studies that
81 burned an additional twenty-five taxa. This work presents statistical analyses of a suite of 13
82 PAHs (Fig. 1) from 32 plant taxa, representing a total of 56 samples generated under different
83 experimental conditions (Table 1; Table EA1). We examined molecular ratio parameters derived
84 from the literature and based on statistical patterns that emerged from the dataset (Table 2).
85
86 **2. Methods**
87 **2.1 Experimental and chemical analyses (new data)**
88 Experimental conditions and vegetation samples for burn experiments were described by
89 Vitzthum von Eckstaedt et al. (2012). Briefly, dead, dry plant material (a mix of leaves, duff,
90 branches, twigs, and bark) was combusted inside a ventilated tent with an air blower to maintain
91 sufficient ambient O_2 (Vitzthum von Eckstaedt et al. 2012). Ten experiments were conducted with
92 seven different Australian taxa, including two C_4 grasses (*Spinifex* spp. and *Themeda triandra*),
93 one C_3 grass (*Triticum* spp.), two eucalypts (*Corymbia calophylla* and *Eucalyptus diversicolor*),
94 and two gymnosperms (*Ginkgo biloba*, and *Cycas* spp). The two C_4 grasses each were burned
95 twice at slightly different temperatures, while the rest of the plants were each burned once.
96 Temperatures were monitored throughout each experiment as per Vitzthum von Eckstaedt et al.
97 (2012) and maximum recorded temperatures were assigned to each sample. Burn residues were
98 collected and stored in a cool, dry location in glass jars.

Organics were extracted from burn residues *via* Soxhlet extraction (72 hrs) with a 9:1 azeotrope of dichloromethane (DCM) and methanol (MeOH). Approximately 2-10 mg of the extracted bitumen was separated into aliphatic, aromatic, and polar fractions by small-scale silica gel liquid chromatography (Maslen et al., 2011). PAHs were identified and quantified using an Agilent 7890B Gas Chromatograph coupled to a 5977B Mass-Selective detector (GC-MS). The aromatic fraction was injected *via* split-splitless injector (280 °C) operating in splitless mode onto a DB-5ms 60-m column (0.25-mm internal diameter, 0.25-µm film thickness). The oven was held at 60 °C for 2 min, ramped at 4 °C/min to 310 °C and then held for 35 minutes. Samples were run in selective ion monitoring (SIM)/scan mode, which alternates between SIM and full scan modes during a single run (SIM method details in Table A1). Compounds were identified in SIM and full scan mode *via* mass spectra and retention time comparison to authentic standards. PAHs were quantified using selected ions (Table A1) and response factors determined using a 5-pt calibration curve from the same standard PAH suite.

Compound-specific carbon isotope analysis (CSIA) measurements were made with a Thermo Scientific Trace GC Ultra, connected to a Thermo Scientific Delta V Advantage isotope ratio mass spectrometer (irMS) *via* a GC Isolink and Conflo IV. The aromatic fraction was injected into a split-splitless injector operating in splitless mode, held at 280 °C. The same GC conditions used above for GC-MS analyses were used for CSIA. Helium was used as carrier gas at a constant flow of 1.5 mL/min. GC column outflow passed through the GC Isolink combustion reactor (copper oxide and nickel oxide, held at 1000 °C). When concentrations allowed, samples were run in triplicate, and sample standard deviations were generally <0.3‰ (1σ). The $\delta^{13}C$ values were expressed in parts permil (‰) relative to the International Vienna Pee Dee Belemnite (VPDB) standard. Every 2-5 sample measurements, a mixture of standards with known $\delta^{13}C$ values (an in-house mixture of *n*-alkanes from C_{11} to C_{25}, calibrated to the VPDB scale using isotopic reference materials purchased from Arndt Schimmelmann, Indiana University) was

124 analyzed in order to ensure instrument accuracy (0.2‰, 1σ, n=42) and precision (0.2‰,
125 1σ, n=42). Bulk organic carbon isotope measurements on burned and unburned plant material
126 were made with a Thermo Delta V IRMS coupled to a Thermo Elemental Analyzer Flash 1112
127 *via* Conflo IV at the Western Australia Biogeochemistry Centre. Samples were run in duplicate
128 and standard deviations were <0.1‰ (1σ).
129
130 **2.2 Literature data**
131 ***2.2.1 PAH concentration data***
132 Concentrations of 13 PAHs (Fig. 1) generated from burned biomass were compiled from
133 published studies (6 reports; 25 taxa; 46 samples; Oros and Simoneit, 2001a; Oros and Simoneit,
134 2001b; Oros et al., 2006; Wiesenberg et al., 2009; Keiluweit et al., 2012; Santín et al., 2017) and
135 combined with new data (this report; 7 taxa; 10 samples) as described above (Table 1).
136 Additionally, of these studies, 4 reported concentrations of alkylated phenanthrenes, and these
137 were compiled with new data to form a subset of 36 samples to examine alkylated distributions
138 (Table 1). In the last 30 years, there have been many studies measuring PAHs generated from
139 biomass burned under various conditions, and only those samples with the following properties
140 were included in the compilation:
141 1) Concentrations of all 13 PAH compounds were measured *via* GC-MS and reported
142 separately for each compound.
143 2) Samples were derived from a single plant (*i.e.*, not a community or cellulose), using
144 whole biomass (*i.e.,* not a selected tissue like wood), and the taxon was identified
145 3) Highest heating temperature (HTT) was reported (measured or estimated)
146 4) Studies that simulated wood stove burning, rather than vegetation burning, were
147 excluded because these studies used economic wood, which is not representative of
148 wildfires

149 Several studies did not meet one or more of these criteria and thus their results were not
150 included in our analysis (i.e., O' Malley and Burke, 1997; Iinuma et al., 2007; Lu et al., 2009;
151 Wang et al., 2009; Guillon et al., 2013; Wiedemeier et al., 2015b). Even so, our compiled dataset
152 covers a wide variety of plant types (32 taxa) and burn conditions, and allows for statistical
153 analyses to examine potential controls on pyrogenic PAH distributions.
154
155 ***2.2.2 PAH carbon isotope data***
156 Carbon isotope values of phenanthrene, fluoranthene, and pyrene were compiled from
157 two published studies (n=30; O' Malley and Burke, 1997; Guillon et al., 2013), as these
158 compounds tend to dominate parent PAH distributions from biomass combustion(Table 1;
159 Simoneit, 2002). Previous reports found temperature did not exert a significant influence on $\delta^{13}C$
160 values of PAHs (O'Malley et al., 1994; O' Malley and Burke, 1997). As a result, we focused on
161 the influence of plant functional type on $\delta^{13}C$ values of PAHs.
162
163 ***2.2.3 Experimental apparatus***
164 Authors used different experimental approaches to create burn conditions and capture
165 products. Five studies set fire to vegetation under open atmospheric conditions meant to simulate
166 natural fires (Oros and Simoneit, 2001b, 2001a; Oros et al., 2006; Santín et al., 2017; this study).
167 Three studies charred samples using a muffle furnace (Wiesenberg et al., 2009; Keiluweit et al.,
168 2012; Santín et al., 2017). Studies that provided isotope data employed either a fireplace (Guillon
169 et al., 2013) or a combustion furnace (O' Malley and Burke, 1997). O_2 conditions were
170 designated based on reports of experimental setup. Studies that burned under open atmosphere or
171 ventilation were designated "atmospheric" (This study; O' Malley and Burke, 1997; Oros and
172 Simoneit, 2001a; Oros and Simoneit, 2001b; Oros et al., 2006; Guillon et al., 2013; Santín et al.,
173 2017) and studies which noted that samples were burned under O_2-limited conditions were

designated as "O_2-limited" (Wiesenberg et al., 2009; Keiluweit et al., 2012; Santín et al., 2017). None of the studies specified packing or arrangement of the fuel beds. Physiochemical properties (such as porosity and aromaticity) of burn products can differ between natural and laboratory conditions (Santín et al., 2017). In previous individual reports, PAH concentrations and distributions appeared to be less influenced by experimental apparatus and were more dependent on fuel type and temperature (Santín et al., 2017). We assessed this with our larger compilation of new and published data representing molecular and isotopic properties of PAHs under a wide variety of experimental conditions (Table 1).

2.2.4 Designation of burn phase

Samples were collected as either smoke (including air-borne gases, aerosols, and particles) from burn emissions or as solid residues. Smoke samples were collected *via* filtration or condensation (O' Malley and Burke, 1997; Oros and Simoneit, 2001b; Oros and Simoneit, 2001a; Oros et al., 2006; Guillon et al., 2013). Residue samples included all charred material left behind after combustion (this study; Wiesenberg et al., 2009; Keiluweit et al., 2012; Santín et al., 2017). Residues are typically dominated by larger charcoal and ash particles (μm-mm), while smoke samples tend to include mostly small soot and black carbon particles (2-50 μm; Masiello, 2004).

2.3 Statistics

2.3.1 Significance tests

All statistical analyses were conducted in the programing environment of R (R Core Team, 2019). Kruskal-Wallis tests were used to evaluate if concentrations differed under different burn conditions (Hollander and Wolfe, 1973). This metric was chosen because concentration data spanned several orders of magnitude, thus the normal distribution assumption of an ANOVA test would be invalid. Kruskal-Wallis tests assume homoscedasticity, that is, all groups have equal

variances (Hollander and Wolfe, 1973). Levene's test (Levene, 1960) revealed all conditions had p-values >0.01, confirming both homogeneity in variances and that Kruskal-Wallis tests could be used for this dataset.

2.3.2 Generalized multiple linear regression

Multiple linear regression (MLR) was conducted to examine which of the burn conditions had the greatest effect on the residue PAH concentrations. Concentration data was log transformed in order to resemble a normal distribution. Regression was conducted with the burn temperature, O_2 content, and growth form using the 'GLM' function. Since growth form and plant functional type are dependent, plant functional type was excluded from the analysis. Categorical variables were converted to factors for this analysis. Unstandardized coefficients were compared to examine the relative effect of each variable.

2.3.3 Ordination

Non-metric multidimensional scaling (NMDS) was used to examine the main influences on the distributions of PAHs. NMDS is an iterative method that maximizes rank-order correlations in ordination space based on a distance metric (Kruskal, 1964). Many samples had PAHs below detection limits and therefore the datasets are not normally distributed. These "zero" abundance values can distort results in methods that assume normally distributed data (i.e., PCA) but not for parametric methods that use sample rankings (i.e., NMDS;(McCune and Grace, 2002). Prior to NMDS, PAH abundances were logarithmically transformed and individual PAH concentrations were then normalized to the sum total of all PAHs in a sample. NMDS was performed with the Bray Curtis dissimilarity metric and the 'metaMDS' function from the package 'vegan' (Oksanen et al., 2018). Stress was minimized to 0.118, with two convergent solutions after 20 tries. Stress of <0.15 is considered reliable (McCune and Grace, 2002). R^2 values between ordination distance and dissimilarity were 0.95 for a linear fit and 0.99 for a non-metric fit, indicating the method maximized dissimilarity in the dataset. The function 'envfit'

224 from the package 'vegan' was used to interpret the NMDS by testing correlations between the
225 measured experimental conditions and the ordination of samples in multiple dimensions
226 (Oksanen et al., 2018). Additionally, Spearman's rank correlations (ρ) were conducted between
227 NMDS axis scores and each variable to examine which experimental conditions correlated with
228 each axis. The significance of these correlations was evaluated using a repeated permutation test
229 (n=1000; Oksanen et al., 2018).

230 **2.4 Molecular Ratios**

231 We evaluated the utility of indices and molecular ratios based on published studies and also
232 proposed new molecular indices based on patterns that emerged from statistical analyses of data
233 in this study. Because the data used in these metrics are relatively straightforward to determine by
234 GC-MS analyses, they offer potentially useful ways to assess sources of PAHs in sedimentary
235 records.

236

237 ***2.4.1 Alkylated PAH derivative index (APDI)***

238 Alkylated homologs of phenanthrene are widely used to distinguish PAH petrogenic
239 inputs (Laflamme and Hites, 1978; Stogiannidis and Laane, 2015; Rocha and Palma, 2019).
240 Generally, authors use normalized distributions that do not take all of the information from a full
241 distribution into account (i.e., Pyrogenic Index, MP/P; Wang et al., 1999; Yunker et al., 2002;
242 Stogiannidis and Laane, 2015; Rocha and Palma, 2019). Typically, the number of methyl groups
243 decreases for pyrogenic samples, yielding a convex-up shape, while alkylated forms in petrogenic
244 samples define a rising, concave-up curve (Blumer and Youngblood, 1975; Stogiannidis and
245 Laane, 2015). Here, the zero- to tri-methylated phenanthrene distributions were fit to a parabolic
246 function. The function direction and shape are described using its first ($f'(x)$) and second
247 derivatives ($f''(x)$), respectively. For a parabolic curve:

248 $$f(x) = ax^2 + bx + c$$

249

250 if $f'(x) = 2ax + b > 0$, the alkylated profile trends upward (increases)

251 if $f'(x) = 2ax + b < 0$, the alkylated profile trends downward (decreases)

252

253 if $f''(x) = 2a > 0$, the profile is convex up

254 if $f''(x) = 2a < 0$, the profile is concave up

255

256 Alkylated PAH Derivative Index (APDI) takes into account both shape and direction of the
257 profiles for zero-to-three methylated phenanthrenes (Table 2):

258 $[f''(x) - f'(2)] = APDI$

259 APDI values are negative for petrogenic samples (concave, increasing) and positive for pyrogenic
260 profiles (convex, decreasing). APDI can also be applied to other alkylated homologs (i.e., pyrene,
261 and chrysene).

262

263 ***2.4.2 Dimethylphenathrene (DMP) ratios***

264 Dimethyl phenanthrenes (DMP) originate from degradation of softwoods (conifers),
265 hardwoods (angiosperm trees), and grasses (Simoneit, 1986; Benner et al., 1995; Kappenberg et
266 al., 2019). To evaluate DMP products for the plant types and experimental conditions in this
267 study, we used the two ratios reported in Table 2 (Kappenberg et al., 2019).

268

269 ***2.4.3 Size distribution ratio (LMW/Total)***

270 PAHs molecule size aligned strongly along NMDS 1 (Fig. 2a), with the largest PAHs (6
271 rings) to the smallest (3 rings) running from negative to positive values on this axis. Based on this

strong gradient, we defined the ratio LMW/Total (Table 2), and evaluated how well this potential proxy captured the influence of burn phase and other conditions on molecular size distributions.

2.4.4 Retene ratio (Ret/3-ring)

The alkylated three-ringed PAH, retene, is a known gymnosperm burn product. It strongly separated out from other 3-ringed PAHs on the NMDS 2 axis (Fig. 2a). Based on this pattern, we defined the ratio Ret/3-ring (Table 2), and evaluated its utility as a source proxy for gymnosperm burn products.

3. Results

3.1 Concentrations relative to fuel (smoke) and extracted material (residues)

Two quantitative measures of PAH abundances are found in published studies: fire scientists report burn products as emission factors, while organic geochemists report compounds relative to the mass of extracted material. In the published data compiled for this study, PAHs in residues were reported relative to the burned material (ng/g material extracted; Wiesenberg et al., 2009; Keiluweit et al., 2012), while those in smoke were expressed relative to the initial biomass (ng/g material combusted; Oros and Simoneit, 2001a). Thus, we treated mass-normalized compound quantities in each phase separately (Fig. 3; discussed below) and compared prominent compounds normalized to total PAHs in each phase (Section 3.2.1). More speculatively, we estimated emission factors for residue PAH for comparison with published smoke data (discussed in Section 4.1.3).

In residues, total parent PAH concentrations spanned five orders of magnitude (10-10,000 ng/g extracted) and averaged 2203 ng/g, with a median of 442 ng/g (Fig. 3a). Abundances were most strongly influenced by burn temperature (Kruskal-Wallis, $p<0.001$; MLR, coefficient=0.89; Fig. 4b), followed by oxygen limitation (Kruskal-Wallis, $p<0.05$; MLR, coefficient=0.69; Fig. 3c). Residues from burns at temperatures between 300-600°C contained an

297 order of magnitude higher PAH concentrations (500-5000 ng/g) than residues from cooler
298 (<300°C; 50-500 ng/g) or hotter (600°C; 10-100 ng/g) burns (Fig. 2b; Fig. 3). PAH
299 concentrations (log values) had a quadratic relationship with temperature ($R^2 = 0.26$, $p<0.005$)
300 and a maximum (10^4) at 500 °C (Fig. 3b). The influence of temperature persisted for different
301 fuel types (woody or grassy) and for O_2 limited conditions (Fig. 4d; Fig. 4e; Fig. 4f), although
302 correlations were no longer statistically significant due to a reduction in sample size. Notably, the
303 influence of temperature was not present for burns under atmospheric O_2 conditions (Fig. 4c).
304 In smoke samples, parent PAH concentrations spanned five orders of magnitude (10-
305 10,000 ng/g combusted), averaged 7451 ng/g (Fig. 3a), with a median of 5242 ng/g (Fig. 3a). Fuel
306 type had a significant ($p<0.001$) effect on PAHs concentrations (Fig. 4. Woody smoke samples
307 contained an order of magnitude (5000-10,000 ng/g) more PAHs than grass samples (500-1000
308 ng/g; Fig. 3d).
309
310 **3.2 Relative Abundances and Dominant Compounds**
311 Quantities of each compound were normalized to the total 13 compounds targeted for
312 study. Phenanthrene was the most abundant compound in about half of the angiosperm samples,
313 and either pyrene or fluoranthene were most abundant in the other half (Fig. A1). Gymnosperm
314 samples were dominated mostly (50%) by retene and sometimes (35%) by phenanthrene (Fig.
315 A1).
316 NMDS analysis revealed robust patterns among individual PAHs and samples. Plant
317 functional type, burn phase, and O_2 conditions all correlated with PAH distributions ($r^2 = 0.37$,
318 $p<0.001$; $r^2 = 0.24$; $p<0.001$; $r^2 = 0.20$, $p<0.01$), while highest temperature of the burn (HTT) did
319 not ($r^2 = 0.08$, $p=0.152$). In addition to the strong gradient in PAH size along NMDS-1, values on
320 this axis also significantly correlated with sample burn phase ($\rho = -0.48$, $p<0.001$; Fig. 2), with
321 the largest PAHs prevalent in residues and the smallest in smoke. Oxygen levels also correlated

with NMDS-1 values (ρ = -0.52, $p<0.001$). Retene had a distinctively negative NMDS 2 score. Notably, plant functional type significantly correlated to NMDS 2 (ρ = -0.66 $p<0.001$; Fig. 2), and woody gymnosperm samples all fell on the negative side of NMDS 2 (Fig. 2). We reevaluated the NMDS after removing retene to test for PAH distributions that may have been masked by the strength of its signal (Fig. A5). Similar to previous studies (Simoneit, 2002; Guillon et al., 2013), when retene was excluded, plant functional type no longer correlated well to parent PAH distributions (r^2 = 0.11, $p > 0.06$).

3.3 Alkylated phenanthrene distributions

As all samples in this study were produced by combustion of plants, they were expected to display the distinctive "staircase" distributions of declining abundance from 0- to 3-methyl groups (Blumer and Youngblood, 1975; Stogiannidis and Laane, 2015) and positive values of the alkylated PAH derivative index (APDI). This was the case for over 75% of the samples (Fig. 5a; Fig. 5c). Interestingly, ~25% of the samples did not display the typical pyrogenic pattern (Fig. 5b). Anomalous alkylation patterns were not related to temperature, oxygen, or burn phase, and were mostly associated with woody gymnosperm samples (conifers; Fig. 5b). We caution that burns fueled by conifers can produce alkylation patterns and APDI values that appear "petrogenic".

3.4 PAH Carbon isotope ratios

$\delta^{13}C$ values of individual PAHs ranged between -32.0‰ and -14.1‰ (Fig. 6a) and differed as expected for C_4 and C_3 plants (~12‰; Fig. 6). Values for PAHs derived from C_4 plants ranged between -14.1‰ and -17.5‰. Among the C_3 plant samples, PAH from grasses were generally the most ^{13}C-depleted (-30‰), woody plants were intermediate, and those from C_3 shrubs the most enriched (-26‰; Fig. 6b; Fig. 6c; Fig. 6d). PAHs from C_3 woody angiosperms

347 were generally more depleted in ^{13}C than those from C_3 woody gymnosperms (Fig. 6). There
348 were no isotopic trends among the 3-ring and 4-ring PAHs within samples (Fig. 6).
349 Fractionation factors ($\varepsilon_{PAH\text{-}Plant}$, ‰) were calculated to determine the isotopic difference
350 between unburnt biomass and individual compounds (Coplen, 2011; Fig. 7):
351

$$\varepsilon_{PAH\text{-}Plant} = \left(\frac{\delta^{13}C_{PAH}+1}{\delta^{13}C_{plant}+1} - 1\right)$$

352 PAHs produced from burned C_3 woody samples were enriched relative to biomass (ε_{ave} =
353 3.9‰), while PAHs from C_3 and C_4 non-woody fuels differed little from biomass values (ε_{ave} = -
354 0.1 ‰; Fig. 7). There were no systematic trends related to ring size (Fig. 7).
355
356 **4. Discussion**
357 Here, we discuss how the results of this analysis may improve interpretations of PAHs in
358 the sedimentary record. We address the aims of this study by identifying which burn conditions
359 may bias PAH production (4.1), how fuel source and transport processes imprint information on
360 molecular distributions (4.2), and if burn process fractionation impacts the fuel source signals
361 preserved in PAH carbon isotope values (4.3).
362
363 **4.1 Are PAH abundances a useful proxy for fire occurrence?**
364 ***4.1.1 PAH production is biased towards average burn temperatures***
365 PAH production in residues, particularly for O_2-limited burns, is maximized between
366 400-500 °C (Fig. 3b; Fig. 4). In contrast, temperature did not significantly affect PAH
367 concentrations for samples burned exclusively under atmospheric conditions (Fig. 4c),
368 presumably because O_2 was readily available and combustion more efficient.

369 The temperature sensitivity observed in our study is consistent with previous
370 observations (e.g., Keiluweit et al., 2012; McGrath et al., 2003) that PAHs are formed *via*
371 different pathways along a temperature continuum. At low temperatures (< 400°C), dehydration
372 dominates small PAH formation (Simoneit, 1998; Keiluweit et al., 2012), while at higher
373 temperatures (>500°C) free radical condensation dominates (Simoneit, 1998; McGrath et al.,
374 2003; Lima et al., 2005). These processes produce a thermal "sweet spot." At low temperatures,
375 PAH yield is low because small (≤ 2 ring) PAHs are not fully condensed, and at high
376 temperatures, PAHs are either incorporated into larger aromatic particles (>8 rings) or fully
377 combusted. At 500 °C, both processes likely take place and form an amorphous char consisting
378 mostly of mid-sized PAHs (3-7 rings) and other dehydrated alteration products, thus maximizing
379 PAH yields (Keiluweit et al., 2010; Keiluweit et al., 2012).
380 PAH concentrations in sedimentary records are potentially biased toward average
381 wildfire temperatures, which typically occur between 300 and 600 °C (mid-range; Wright and
382 Bailey, 1982; Wolf et al., 2013). Fires that burn at either extremely low (<300 °C) or high (>600
383 °C) temperatures are likely underrepresented in molecular archives.
384 Production bias may result from large shifts in fire type (Scott, 2000). For example,
385 decreased PAH concentrations may reflect a transition from predominately flaming forest fires to
386 smoldering peat fires, rather than less fire occurrence. The use of a fire temperature proxy, such
387 as inertinite reflectance in charcoal or benzene polycarboxylic acid ratios may be one way to
388 identify if a paleofire burned at an extreme low or high temperatures that could have biased PAH
389 production (Conedera et al., 2009; Kappenberg et al., 2019).
390

391 ***4.1.2 Fuel bias and biomass-normalized abundances***

392 Burns of woody vegetation produced an order of magnitude more PAHs in smoke than
393 grassy vegetation (Fig. 3; Fig. 4d). Further, woody ecosystems produce significantly more above-
394 ground biomass than grasslands (Whittaker and Likens, 1973), even though grassland systems
395 generally burn much more (10-100x) frequently than most forest biomes (Archibald et al., 2013).
396 Normalizing PAH concentrations to a plant biomarker (e.g., *n*-alkanes or terpenoids) can help
397 partially account for this PAH production bias (Denis et al., 2017; Karp et al., 2018), assuming
398 the plant biomarker reasonably represents burned biomass.

399 Plant biomarkers are subject to transport and production biases. For example, certain leaf
400 waxes are preferentially produced by different plant types (Freeman and Pancost, 2014;
401 Diefendorf and Freimuth, 2017) and differential transport between PAHs and biomarkers can
402 have additional effects (Denis et al., 2017). Future core-top calibration studies could help
403 constrain these considerations for both fire and plant biomarkers, particularly if combined with
404 data for plant communities and fire histories.

405 Despite remaining uncertainties, PAH-plant biomarker normalization was successfully
406 used in studies that examined fire ecology changes during the Neogene. PAH amounts
407 normalized to a plant biomarker increased by an order of magnitude and were highly correlated
408 with evidence for C_4 grass inputs (Karp et al., 2018). These results suggest the PAH production
409 bias between wood-smoke and grass-smoke does not impede grass fire records when normalized
410 and integrated over deep timescales and for major ecosystem transitions.

411 The potential for wood smoke inputs to obscure a grass-associated increase in fire
412 occurrence likely depends on the duration of time integrated in a record. Higher-resolution
413 temporal records may be more susceptible to source-related production bias, as they include
414 fewer individual fire events. Plant-biomarker-normalized PAH concentrations may be particularly

415 useful for reconstructing grassland fires, as charcoal from grass tends to be underrepresented in
416 sedimentary records (Hilscher and Knicker, 2011; Leys et al., 2017).
417
418 ***4.1.3 Amounts of PAH estimated in smoke vs. solid residues***
419 Available data for PAH abundances were normalized differently for smoke and for solid
420 burn residues, which prevented direct comparison between the two phases. To get around this
421 challenge, we estimated PAH residue emission factors (ng/material combusted) using some
422 simple assumptions and mass loss constraints published in the literature (Czimczik et al., 2002;
423 Collura et al., 2005).
424 Based on the burn temperature and plant functional type for each sample, we assigned a
425 % mass loss relative to the initial unburnt fuel using thermogravimetric data from experimentally
426 burned softwood (Czimczik et al., 2002), hardwood (Czimczik et al., 2002), and grass (Collura et
427 al., 2005) chars. The loss term was converted to a mass ratio of residue/total unburnt biomass,
428 which was then multiplied by measured PAH concentrations normalized to material extracted
429 (ng/g). This converted PAH concentrations into units of ng/g unburnt material, which
430 approximates estimated emission factors for residue samples so they can be compared with
431 smoke data.
432 Parent PAH concentrations in the residues had significantly lower emission factors than
433 smoke (<0.001; Fig. 8). Residue parent PAH concentrations averaged 1214 ng/g material
434 combusted, which is 7x less than the average for smoke (7451 ng/g material combusted). If this
435 difference in emission factors is representative for natural burns, then PAH records mostly
436 represent smoke inputs relative to char residues. This inference is consistent with environmental
437 studies that found PAHs and other char parameters were decoupled in recent sedimentary records
438 (Denis et al., 2012; Hanke et al., 2016; Hanke et al., 2017), and that PAH concentrations were

more strongly associated with soot than chars (Han et al., 2015). We caution field observations may be influenced by fossil fuel combustion (Hanke et al., 2016).

Future studies in regions not impacted by anthropogenic air pollution will strengthen our understanding of the degree to which regional signals are recorded by smoke-derived PAHs, and local fire patterns are recorded by charcoal in the same sedimentary record (Hanke et al., 2017; Miller et al., 2017). We recommend future studies directly compare PAH emission factors (ng/g biomass burned) for both smoke and residues. This normalization is particularly useful for paleo-proxy comparisons that normalize PAH concentrations to proxies for plant biomass.

4.2 What factors are reflected in PAH distributions?

4.2.1 PAH size distributions linked to physical properties and burn phase, but not fire temperature

Previous authors have suggested fire temperature (McGrath et al., 2003; McBeath et al., 2011; Wiedemeier et al., 2015b) and O_2 content (Lima et al., 2005) significantly determine PAH molecular distribution patterns. Changes in sedimentary PAH size distributions have been attributed to changes in fire temperature and intensity (Denis et al., 2012). However, this interpretation is not supported by this or previous studies (Lima et al., 2005) in which PAH distribution patterns were most strongly linked to the burn phase (residue or smoke; Fig. 2). The pronounced PAH size difference between smoke and residues provides a useful means to estimate which burn phase contributed PAHs to a sedimentary record. Further, size sorting of either water-borne or air-borne smoke and char particles has potential to imprint on PAH distributions as they are transported and deposited in sediments.

PAHs in smoke can persist in the gas phase, although larger forms will sorb to particles (Dachs and Eisenreich, 2000; Han et al., 2010; Jenkins et al., 1996; Shen et al., 2011). In contrast, solid residues include a full range of PAH structures including condensed high-molecular-weight

464 PAHs (McGrath et al., 2003; Lima et al., 2005). Larger PAHs (with low V_p, C_w^{sat}, and high K_{ow})
465 will sorb primarily to organic residues in the solid phase and are less likely to volatilize and
466 subsequently sorb to airborne particles.

467 Because they mostly reflect molecular size, molecule NMDS 1 scores had strong log-
468 linear relationships with K_{ow}, V_p, and C_w^{sat} values (Fig. 9). This suggests NMDS 1 scores reflect
469 these physical properties, rather than simply size of the molecule. For example, NMDS 1 scores
470 break between two pairs of 4-ringed compounds: the more condensed pyrene and fluoranthene
471 (Py, Flu; MW 202) and the more linear-shaped benz[*a*]anthracene and chrysene (Chry, BaA; MW
472 228). Chemical properties for the two pairs of structures strongly differ: three orders of
473 magnitude in V_p, two orders of magnitude in C_w^{sat}, and an order of magnitude in K_{OW} (Fig. 9).
474 Many studies sort PAHs by numbers of rings (e.g., Dong et al., 2012; Han et al., 2015; Callegaro
475 et al., 2018; Rocha and Palma, 2019), even though physical properties dictate PAH solubility,
476 volatility, and other behaviors in the environment (Fraser et al., 1998; Lima et al., 2005). We
477 recommend proxy tools involving PAH are based on solubility and other physical or chemical
478 properties rather than on the number of rings. For example, due to their different shapes (which
479 set both molecule surface areas and molecular volumes), the physicochemical properties of Flu
480 and Pyr are similar to 3-ring PAHs, and those of Chry and BaA are similar to 5-ring PAHs (Fig.
481 9). So, while Flu and Pyr were prominent in smoke along with other 4-ring forms (Fig, A2), Chry
482 dominated PAH in residues (Fig. A2).
483
484 4.2.2 ***PAH size distributions also reflect transport***
485 We suggest the LMW/Total ratio in sedimentary archives can potentially distinguish
486 relative smoke and char inputs and incorporate the influence of transport. Based on NMDS
487 results, we defined the LMW/total ratio (Table 2) to represent PAH with masses ≤202 AMU
488 relative to total parent PAHs (Fig. 1 for abbreviations), similar other studies (Stogiannidis and

Laane, 2015). The ratio ranged between 1.00 and 0.75 (μ=0.85) in smoke samples and was lower in residues, ranging between 0.40 and 0.80 (μ=0.64; Fig. 10a). Calculated LMW/Total for environmental data reported in the literature (Olivella et al., 2006; Alves et al., 2011; Vicente et al., 2011; Vicente et al., 2012; Harper et al., 2019) for smoke (μ=0.75, n=6) and residues (μ=0.65, n=9) fell within ranges observed in this study.

Smoke particles are emitted into the troposphere, aerially transported, and travel far from the source (Ferrare et al., 1990). Char can also be emitted into the troposphere, where transport distances depend on the particle size and shape (Peters and Higuera, 2007; Vachula and Richter, 2017). Char residues are subject to secondary transport *via* wind, water, or soil processes, or they can be stored in soils before being remobilized to downstream sediment archives (Conedera et al., 2009; Santín et al., 2016; Hanke et al., 2017). While uncertainties remain in constraining charcoal transport and incorporation into sedimentary archives (Conedera et al., 2009; Vachula and Richter, 2017), char residues generally remain closer to the site of production (Bird et al., 2015), and record more localized fire events (Conedera et al., 2009).

Due to size differences between char particles (10-100s μm) and fine aerosol particles (<2.5 μm) in smoke, char particles are typically transported several orders of magnitude shorter distances (10^{-2}-10 km; Peters and Higuera, 2007; Vachula and Richter, 2017) than smoke aerosols (10^{2}-10^{4} km; e.g.,Wu et al., 2018; Sicard et al., 2019). In the environment, volatile LMW PAHs are deposited further from a combustion source while particle-associated HMW PAHs are deposited closer to the source (Halsall et al., 2001; Ma et al., 2013). In soils, HMW PAHs are present in higher concentrations closer to point pollution sources as indicated by their correlation with black carbon deposition (Nam et al., 2008; Nam et al., 2009; Han et al., 2015).

4.2.3 ***PAH size distributions can be modified by biodegradation***

513 The biodegradation rate of PAHs in the environment is controlled by aqueous solubility, ,
514 and LMW PAHs are highly susceptible to loss (Fig. 9a; Fig. 9c; Lima et al., 2005; Stogiannidis
515 and Laane, 2015; González-Gaya et al., 2019). Alkylated forms are less susceptible to
516 biodegradation (Stogiannidis and Laane, 2015; Kang et al., 2016) because they are less soluble
517 than parent PAHs and the methyl sites hinder biodegradation initiated by ring hydroxylation
518 (Mallick et al., 2011). Biodegradation will therefore increase the LMW/total ratio and shift the
519 APDI metric toward more negative values. Although more studies are needed, anomalous APDI
520 values may help identify the influence of degradation on PAH size distributions, while
521 complimentary sedimentary (i.e., mineralogical and grain size analyses) and bulk black carbon
522 (i.e., size and concentration measurements) data can also strengthen interpretations of
523 LMW/Total as an indicator of changing smoke and residue inputs.
524
525 ***4.2.4 Alkylated PAH distributions mostly reflect plant type***
526 Unlike parent PAH distributions (Lima et al., 2005; Stogiannidis and Laane, 2015),
527 retene can serve as an indicator of plant type burned in a fire. A degradation product of abietic
528 acid, retene is a marker of burn products from conifers (Simoneit, 1977; Wakeham et al., 1980;
529 Oros and Simoneit, 2001a). We defined Ret/3-ring to highlight this source signal by accounting
530 for the potential influence of burn phase, transport, and biodegradation. Angiosperm samples had
531 consistently low Ret/3-ring values (<0.1), while gymnosperm values were higher, but ranged
532 widely (0.2-0.8; Fig. 10b). We suggest low Ret/3-ring values generally identify burned plant
533 communities in which conifers were rare. Interpretations may be checked by cross plotting or
534 calculating correlation coefficients of Ret/3-ring with other proxies for gymnosperms relative to
535 angiosperms, such as the diterpenoid to *n*-alkane ratio (Diefendorf et al., 2014) or pollen analyses.
536 In this study, as in previous reports, dimethyl phenanthrenes (DMP) highly correlated
537 with plant functional types, consistent with their known origin as degradation products of

softwoods (conifers), hardwoods (angiosperm trees), and grasses (Fig. 11; Simoneit, 1986; Benner et al., 1995; Kappenberg et al., 2019). DMP isomers associated with softwoods are usually sourced from Pinaceae, rather than gymnosperms more generally (Yunker et al., 2002; Kappenberg et al., 2019). Consistent with this, both DMP ratios for *Ginkgo biloba* sorted with the hardwood samples, even though it is a cone-producing gymnosperm (Fig. 11). Ratios for *Triticum spp.* were lower than reported by Kappenberg et al. (2019) and plotted with the hardwood samples (Fig. 11). Additionally, the DMP-x ratio for one eucalypt plotted with the grass samples (Fig. 11). DMP-x ratios between 0.55 and 0.7 may reflect mixed hardwood and grass inputs. These differences from the initial ranges suggested in Kappenberg et al. (2019) highlight the need for additional studies with more diverse plant types to improve classifications from these ratios. Regardless, DMP-x, DMP-y, and Ret/3-ring ratios are promising tools to track combusted plant communities in sedimentary records.

While most samples in this study had the expected pyrogenic distributions for alkylated phenanthrenes (Fig. 5a), several conifers did not (Fig. 5b). Conifers produce triterpenoids that share the 3-ring structure of phenanthrene, such as abiatanes, pimaranes and tetracyclics (Simoneit, 1986; Diefendorf et al., 2019). Degradation products such as 1,7-dimethylphenanthrene and 1,2,8-trimethylphenanthrene have been attributed to the alteration of pimarane and phyllocladane (Simoneit, 1977; Simoneit, 1986; Budzinski et al., 1995; Benner et al., 1995; Grice et al., 2001; Oros and Simoneit, 2001a; Yunker et al., 2002; Stogiannidis and Laane, 2015). We suggest anomalously elevated alkyl phenanthrene distributions (negative APDI values) can reflect a conifer source rather than petrogenic PAHs, and can be checked using the Ret/3-ring ratio.

561 **4.3 How do fuel and burn process imprint $\delta^{13}C$ values of PAHs?**

562 PAH carbon isotope values strongly reflected their burned plant sources, consistent with
563 previous reports (Fig. 6; O'Malley et al., 1994; O' Malley and Burke, 1997). C_3 plants display a
564 broad range of carbon isotope values (Deines, 1980; Farquhar et al., 1989; Tipple and Pagani,
565 2007; Diefendorf and Freimuth, 2017), reflecting the influence of environmental (i.e., water
566 availability, pCO_2, light) and biological (i.e., taxonomy) variables (Diefendorf et al., 2010;
567 Graham et al., 2014). Similarly, C_3-derived PAHs varied by ~8‰, while C_4-derived PAHs fell
568 within a narrow range (~3‰). PAHs from woody angiosperms were 1-3‰ more depleted in ^{13}C
569 than those from woody gymnosperms (Fig. 6), consistent with isotope differences observed for
570 these plant groups (Leavitt and Newberry, 1992; Diefendorf et al., 2010). PAHs from C_3 grass
571 were the most depleted in ^{13}C among all C_3 plant types (Fig. 6), consistent with C_3 grass biomass
572 values (Arens et al., 2000).
573
574 4.3.1 ***Minimal fractionation during production of PAH in residues***
575 Fractionation factors enabled us to compared $\delta^{13}C$ measurements between individual
576 molecules and plant material used in the burns. The $\varepsilon_{PAH\text{-}plant}$ values for PAHs from from all plants
577 analyzed in this study were generally within plus or minus one permil (±1‰; Fig. 7), with no
578 systematic direction. We note that because mostly leaves were archived, bulk biomass isotope
579 values from woody plants underrepresent carbon from wood. There is little difference between
580 leaf and wood for most plants, although this is not true for Eucalypts, for which wood is ~3‰
581 more enriched than leaves (Schulze et al., 2006). Thus, epsilon values for Eucalypts were
582 corrected assuming a wood-to-leaf mass ratio of 9:1 (Ribeiro et al., 2015). When this correction
583 was applied, $\varepsilon_{PAH\text{-}plant}$ values for all PAHs were ± ~1‰ (Fig. 7). C_4 non-woody pyrene was the
584 only exception, with a slightly greater $\varepsilon_{PAH\text{-}plant}$ value (1.6‰; Fig. 7). PAHs form through radical

585 reactions and condensation of organic fragments at high temperatures (Richter and Howard,
586 2000). The close isotopic relationship between biomass and PAHs indicate that the molecular
587 fragments were not derived from an isotopically distinct compound class or fractionated during
588 condensation.
589
590 4.3.2 ***Potentially variable fractionation during production of PAH in smoke***
591 In contrast to our finding for residue samples, O'Malley and Burke (1997) observed
592 PAHs in smoke were ~2‰ depleted relative to plant biomass (Fig. 7) and proposed that PAHs
593 were preferentially sourced from lignin. In published studies, $\delta^{13}C$ values of bulk residues were
594 similar to plant biomass (<1‰), while values for bulk aerosol carbon were variable (1-7‰),
595 particularly for C_4 plants (Turekian et al., 1995; Turekian et al., 1998). Preferential volatilization
596 of ^{13}C-depleted, labile components (Turekian et al., 1998) or as originally suggested, isotopic
597 distinctions among the sources (such as lignin) for radicals that form PAHs in the smoke phase
598 potentially account for isotopic depletion in smoke PAHs observed by O'Malley and Burke
599 (1997).
600 Surveys of bulk carbon isotope work on pyrogenic carbon also indicate that O_2 content
601 and temperature may impact the magnitude of fractionation due to differential loss of ^{13}C
602 enriched cellulose (Bird and Ascough, 2012 and references herein). While environmental studies
603 suggest O_2 and temperature do not influence PAH $\delta^{13}C$ values (O'Malley et al., 1994; Holman
604 and Grice, 2018), more work is needed, given only two studies to date (this study and O' Malley
605 and Burke, 1997) have measured $\delta^{13}C$ of both PAHs and the unburnt plant material.
606
607 ***4.3.3 An approach to reconstructing burned biomass by isotope mass balance***
608 Isotopic records of bulk pyrogenic carbon phases are widely used to reconstruct changes
609 in plant community burning (e.g., Shen et al., 2018; Bird et al., 2019), but this technique is

610 complicated by preferential loss, heterogeneity, transport, and preservation (Turekian et al., 1998;
611 Bird and Ascough, 2012; Saiz et al., 2015). While compound-specific isotope measurements are
612 more analytically intensive, they eliminate some of the uncertainties associated with mixed bulk
613 isotope measurements (Freeman and Pancost, 2014). The large differences between PAHs
614 derived from C_3 and C_4 plant biomass and low fractionation between PAHs and unburned
615 biomass indicate that PAHs have great potential to serve as a proxy for burned vegetation in
616 sedimentary records.

617 However, because of production biases, it is not straightforward to use PAH isotope
618 abundances to estimate relative contribution of C_3 woody and C_3 grass fuels to paleo wildfires.
619 Wood-derived smoke contains a higher abundance of PAHs (Fig. 3; Fig. 4d), while PAHs from
620 grass ecosystems can be elevated because they burn more frequently than forests. Additionally,
621 C_3 grasses had more negative $\delta^{13}C$ values than woody plants, which may negatively skew C_3
622 endmembers. General, large-scale shifts in C_3 and C_4 burning through time can be derived with
623 carbon isotope measurements of PAHs in sediments. Isotope data can be compared with alkylated
624 PAH ratios, such as DMP-y, as well as to source-specific plant biomarkers (based on lignin
625 monomers, alkane distributions or terpenoid biomarkers; Freeman and Pancost, 2014) to help
626 constrain plant sources. Uncertainties in relative production is a problem that many paleo proxies
627 (i.e., *n*-alkanes, pollen) must address in order to translate into quantitative estimates of plant types
628 on a landscape.

629

630 **6. Conclusions**

631 This work evaluated the amounts, distributions, and isotopic signatures of PAHs
632 produced from burned plant samples. Relative to burned biomass, estimated emission factors for
633 PAHs in smoke are many times greater than for char, such that inputs to the sedimentary record
634 are biased toward smoke-borne compounds. PAH molecular distributions reflect both plant

635 sources and burn phase, but not burn temperatures. PAH size distributions quantified in NMDS
636 analyses and by LMW/Total ratios reflected structure-specific chemical-physical properties that
637 dictate partitioning between solid residue and smoke burn phases. We caution size distributions
638 can be influenced by particle sorting during transport of burn phases or biodegradation. Alkylated
639 PAHs reflect plant types consistent with previous work. In particular, retene and dimethyl
640 phenanthrene ratios distinguished gymnosperms from angiosperms, and woody angiosperms from
641 grasses and woody gymnosperms. $\delta^{13}C$ values of PAHs were not fractionated relative to plant
642 biomass values, and reflected plant function types and their photosynthetic pathway.
643 Overall, both relative abundances and carbon isotopes of PAHs in the sedimentary record
644 can record burned plant communities, while size patterns reflect burned particle phase and
645 transport (Fig. 12). To reconstruct fire occurrence and account for production biases, sedimentary
646 PAHs abundances in sediment records should be normalized to a plant biomarkers. The
647 framework presented here improves the interpretability of PAHs as a proxy for changes in paleo-
648 fire regimes.
649
650 **Acknowledgements**
651 We gratefully acknowledge funding for this work provided to ATK from the Pennsylvania State
652 Global Programs through a Graduate Student Travel Grant and the European Association of
653 Organic Geochemists (EAOG) through the 2018 EAOG Research Award. ATK was supported by
654 a National Science Foundation (NSF) Graduate Research Fellowship under Grant No.
655 DGE1255832. ATK thanks Sarah Ivory, Elizabeth Hajek, Mark Patzkowsky, and Erica
656 Smithwick for constructive feedback on this manuscript. KG thanks the Australian Research
657 Council (ARC) for support of a Discovery Outstanding Research Award for the burn experiments
658 (#DP130100577) and ARC infrastructure grant # LE110100119 for compound specific equipment.
659 The authors acknowledge Christiane Vitzthum von Eckstaedt and Caroline Jaraula for performing

controlled burn experiments at Curtin University. We thank three anonymous reviewers for constuctive comments and suggestions that greatly improved this manuscript.

Figure Captions:

Table 1: Summary of experimental conditions for included studies. Types of data refer to which type of PAH data was used from each study. Details for each sample available in Table EA1.

Table 2: Ratios and indices used in this study to examine changes in PAH distributions.

Figure **1**: Polycyclic aromatic hydrocarbons (PAHs). Structures, names, and abbreviations of PAHs examined.

Figure **2**: Non-metric multidimensional scaling of PAH distributions from vegetation burning. A) Ordination plot of compound scores ('species scores'). Vectors represent the magnitude and direction the correlation of external variables to NMDS ordination. The table shows the NMDS coordinates, R^2 from 'envfit', ρ from NMDS 1 and NMDS 2, and p-values of these respective

correlations. Significance levels based on a permutation test are as follows: ***<0.001, **<0.01, *<0.1. B) Ordination plot of sample scores interpreted for NMDS 1. Samples are coded by burn phase. The burn phase and O_2 limitation correlation vectors have the strongest association with NMDS 1. C) Ordination plot of sample scores interpreted for NMDS 2. Samples are coded by plant functional type. The plant functional type correlation vector has the strongest association with NMDS 2.

Figure **3**: Total concentrations of parent PAHs produced under different burn conditions. All plots are shown on a logarithmic scale. The white plots on the left side represent smoke samples and are in ng/g material combusted. The grey plots on the right side represent residue samples and are in ng/g material extracted. Significance level for non-parametric tests are as follows: ***<0.001, **<0.01, *<0.1, 'NS' = non-significant and refer to the plot above them. A) Total Smoke and residue total concentrations. Averages are marked by '+' B) PAH concentrations separated out by growth form: Woody (W) and Grass (G). C) PAH concentrations separated by plant functional type. AW = Woody Angiosperms, GW = Woody Gymnosperms, C3G = C_3 Grasses and C4G = C_4 grasses. D) PAH concentrations separated by HTT. Low HTT<300°C, Mid HTT 300°C to 600°C, and high 600°C. E) PAH concentrations separated by samples burned under atmospheric O_2 conditions (21%; 'no' in E) or O_2 limited conditions (<21%; 'yes' in E).

Figure **4**: The distribution of residue parent PAH concentrations over a range of HTT. A) PAH concentrations versus HTT. B) Order of magnitude of PAH concentrations versus HTT. A quadratic fit best describes the relationships between HTT and the order of magnitude of PAHs produced at different temperatures, with a maximum falling at 500°C. R^2 =0.26, p<0.001. C)

705 Atmospheric condition samples separated by HTT. D) O_2 limited samples separated by HTT. E)
706 Woody samples separated by HTT. D) Grass samples separated by HTT.

707 Figure **5**: The alkylated phenanthrene distributions generated from burned vegetation. A) Shaded
708 bars represent the average of the relative amounts of zero to tri-methyl phenanthrenes in samples
709 where the alkylated forms were measured. The error bars are based on 1σ standard deviation. A)
710 Examples of samples that do not display a staircase distribution. B) Examples of samples that
711 display a pyrogenic staircase distribution. P = phenanthrene, MP = sum of methyphenanthrene
712 isomers, DMP = sum of dimethylphenanthrene isomers, TMP = sum of trimethylphenanthrene
713 isomers. Alkylated PAH index (APDI)

714

715 Figure **6**: Carbon isotope distributions of PAHs generated from different types of burned
716 vegetation. A) Carbon isotope distributions of PAHs generated from C_3 and C_4 burning.
717 Compilation of phenanthrene, fluoranthene and pyrene values. B) $\delta^{13}C$ values of pyrene from
718 different plant functional types. C) $\delta^{13}C$ values of fluoranthene from different plant functional
719 types. D) $\delta^{13}C$ values of phenanthrene from different plant functional types. C_3 plots are the
720 combination of the four C_3 plant types that are plotted separately

721

722 Figure **7**: Apparent fractionation (ε) between $\delta^{13}C$ of bulk plant material and $\delta^{13}C$ of PAHs
723 Points are averages, and error bars are based on 1σ standard deviation. ε of PAHs generated from
724 burning of different plant functional types are color coded. Circles represent new measurements
725 generated in this study. Diamonds indicate measurements from O'Malley et al. (1997). Dotted
726 lines indicate average ε for both studies. Open circle indicates woody samples that were corrected

727 to account for bias against woody tissues in the bulk plant material $\delta^{13}C$ measurement.

728

729 Figure 8: Boxplot comparison of PAH emission factors (ng/g material combusted) of burn
730 residues and smoke. Residue emission factors were estimated using %mass loss observations
731 from Czimczik et al. (2002) and Collura et al. (2005). *** indicates p-value<0.001. Averages are
732 marked by '+'

733

734 Figure **9**: Physio-chemical properties of PAHs versus NMDS 1 scores. The y-axes of all plots
735 represent the log properties of PAHs. A) Octanal-water partition coefficients versus NMDS 1
736 values. B) Vapor pressure versus NMDS 1 values. C) Solubility (saturated, in water) versus
737 NMDS 1 values.

738

739 Figure **10**: Diagnostic ratios based on variables identified via NMDS. Significance level for non-
740 parametric tests were all significant at the 0.001 level A) LMW/Total ratio for different burn
741 phases. B) Ret/(Ret+3-ring) ratio of angiosperms versus gymnosperms.

742

743 Figure **11**: Biplot of dimethyl phenanthrene ratios from new samples generated in this study.
744 Boxes are defined by plant functional type ranges set by Kappenberg et al. (2019). Samples are
745 colored by plant functional type. Several samples plot out of the ranges defined by the previous
746 study, which are discussed in section 5.2.2.

747

748 Figure **12**: A visual summary of PAH tools identified in this study that can be used to reconstruct
749 paleo-fire conditions. Ret/3-ring stands for Ret/(Ret+Phen+Ant). DMP-x stands for the DMP

ratio on the x-axis of Fig 10, (1,7-DMP+ 2,6|3,5-DMP)/(1,7-DMP+ 2,6|3,5-DMP+1,2-DMP).

DMP-y stands for the DMP ratio on the y-axis of Fig 10, 1,7-DMP/1,2-DMP.

6. References

Alves C. A., Vicente A., Monteiro C., Gonçalves C., Evtyugina M. and Pio C. (2011) Emission of trace gases and organic components in smoke particles from a wildfire in a mixed-evergreen forest in Portugal. *Sci. Total Environ.* **409**, 1466–1475.

Archibald S., Lehmann C. E. R., Belcher C., Bond W. J., Bradstock R. A., Daniau A.-L., Dexter K., Forrestel E. J., Greve M., He T., Higgins S. I., Lamont B. B., McGlinn D. J., Moncreiff G. R., Osborne C. P., Pausas J. G., Price O., Ripley B. S., Rogers B., Schwilk D. W., Simon M. F., Turetsky M., Van der Werf G. R. and Zanne A. E. (2017) Biological and geophysical feedbacks with fire in the Earth System. *Environ. Res. Lett.*

Archibald S., Lehmann C. E. R., Gómez-dans J. L. and Bradstock R. A. (2013) Defining pyromes and global syndromes of fire regimes. *PNAS* **110**, 6442–6447.

Arens N. C., Hope Jahren A. and Amundson R. (2000) Can C3 plants faithfully record the carbon isotopic composition of atmospheric carbon dioxide? *Paleobiology* **26**, 137–164.

Argiriadis E., Battistel D., McWethy D. B., Vecchiato M., Kirchgeorg T., Kehrwald N. M., Whitlock C., Wilmshurst J. M. and Barbante C. (2018) Lake sediment fecal and biomass burning biomarkers provide direct evidence for prehistoric human-lit fires in New Zealand. *Sci. Rep.* **8**, 2–10.

Benner B. A., Wise S. A., Currie L. A., Klouda G. A., Klinedinst D. B., Zweidinger R. B., Stevens R. K. and Lewis C. W. (1995) Distinguishing the Contributions of Residential Wood Combustion and Mobile Source Emissions Using Relative Concentrations of Dimethylphenanthrene Isomers. *Environ. Sci. Technol.* **29**, 2382–2389.

Bird M. I. and Ascough P. L. (2012) Isotopes in pyrogenic carbon: A review. *Org. Geochem.* **42**, 1529–1539.

Bird M. I., Brand M., Diefendorf A. F., Haig J. L., Hutley L. B., Levchenko V., Ridd P. V, Rowe C., Whinney J., Wurster C. M. and Zwart C. (2019) Identifying the ‘ savanna ’ signature in lacustrine sediments in northern Australia. *Quat. Sci. Rev.* **203**, 233–247.

Bird M. I., Wynn J. G., Saiz G., Wurster C. M. and Mcbeath A. (2015) The Pyrogenic Carbon Cycle. *Annu. Rev. Earth Planet. Sci.*, 273–300.

Blumer M. and Youngblood W.(1975) Polycyclic Aromatic Hydrocarbons in Soils and Recent Sediments. *Science (80-.).* **188**, 53–55.

Bowman D. M. J. S., Balch J. K., Artaxo P., Bond W. J., Carlson J. M., Cochrane M. A., D’Antonio C. M., DeFries R. S., Doyle J. C., Harrison S. P., Johnston F. H., Keeley J. E., Krawchuk M. A., Kull C. A., Marston J. B., Moritz M. A., Prentice I. C., Roos C. I., Scott A. C., Swetnam T. W., van der Werf G. R. and Pyne S. J. (2009) Fire in the Earth System. *Science (80-.).* **324**, 481–484.

Budzinski H., Garrigues P., Connan J., Devillers J., Domine D., Radke M. and Oudins J. L. (1995) Alkylated phenanthrene distributions as maturity and origin indicators in crude oils and rock extracts. *Geochim. Cosmochim. Acta* **59**, 2043–2056.

Burke K. D., Williams J. W., Chandler M. A., Haywood A. M., Lunt D. J. and Otto-Bliesner B. L. (2018) Pliocene and Eocene provide best analogs for near-future climates. *Proc. Natl.*

792 *Acad. Sci.* **115**, 13288–13293.
793 Callegaro A., Matsubara Pereira F., Battistel D., Kehrwald N. M., Bird B. W., Kirchgeorg T. and
794 Barbante C. (2018) Fire, vegetation and Holocene climate in the south-eastern Tibetan
795 Plateau: a multi-biomarker reconstruction from Paru Co. *Clim. Past Discuss.* **5194**, 1–33.
796 Collura S., Azambre B. and Weber J. V. (2005) Thermal behavior of Miscanthus grasses, an
797 alternative biologial fuel. *Environ. Chem. Lett.* **3**, 95–99.
798 Conedera M., Tinner W., Neff C., Meurer M., Dickens A. F. and Krebs P. (2009) Reconstructing
799 past fire regimes: methods, applications, and relevance to fire management and
800 conservation. *Quat. Sci. Rev.* **28**, 555–576.
801 Coplen T. B. (2011) Guidelines and recommended terms for expression of stable-isotope-ratio
802 and gas-ratio measurement results. *Rapid Commun. Mass Spectrom.* **25**, 2538–2560.
803 Czimczik C. I., Preston C. M., Schmidt M. W. I., Werner R. A. and Schulze E. D. (2002) Effects
804 of charring on mass, organic carbon, and stable carbon isotope composition of wood. *Org.*
805 *Geochem.* **33**, 1207–1223.
806 Daniau A.-L. and Brücher T. (2016) Fire, climate and biomes – towards a better understanding of
807 this complex relationship. *Past Glob. Chang. Mag.* **24**, 79–79.
808 Daniau A. L., Bartlein P. J., Harrison S. P., Prentice I. C., Brewer S., Friedlingstein P., Harrison-
809 Prentice T. I., Inoue J., Izumi K., Marlon J. R., Mooney S., Power M. J., Stevenson J.,
810 Tinner W., Andrič M., Atanassova J., Behling H., Black M., Blarquez O., Brown K. J.,
811 Carcaillet C., Colhoun E. A., Colombaroli D., Davis B. A. S., D'Costa D., Dodson J.,
812 Dupont L., Eshetu Z., Gavin D. G., Genries A., Haberle S., Hallett D. J., Hope G., Horn S.
813 P., Kassa T. G., Katamura F., Kennedy L. M., Kershaw P., Krivonogov S., Long C., Magri
814 D., Marinova E., McKenzie G. M., Moreno P. I., Moss P., Neumann F. H., Norstrm E.,
815 Paitre C., Rius D., Roberts N., Robinson G. S., Sasaki N., Scott L., Takahara H., Terwilliger
816 V., Thevenon F., Turner R., Valsecchi V. G., Vannière B., Walsh M., Williams N. and
817 Zhang Y. (2012) Predictability of biomass burning in response to climate changes. *Global*
818 *Biogeochem. Cycles* **26**, 1–12.
819 Deines P. (1980) The isotope composition of reduced organic carbon. In *A Handbook of*
820 *Environmental Isotope Geochemistry, The Terrestrial Environment* (eds. P. Fritz and J.
821 Fontes). Elsevier, Amsterdam, Oxford, New York. pp. 329–406.
822 Denis E. H. (2016) Production and preservation of organic and fire-derived carbon across the
823 Paleocene-Eocene Thermal Maximum. The Pennsylvania State University.
824 Denis E. H., Pedentchouk N., Schouten S., Pagani M. and Freeman K. H. (2017) Fire and
825 ecosystem change in the Arctic across the Paleocene–Eocene Thermal Maximum. *Earth*
826 *Planet. Sci. Lett.* **467**, 149–156.
827 Denis E. H., Toney J. L., Tarozo R., Scott Anderson R., Roach L. D. and Huang Y. (2012)
828 Polycyclic aromatic hydrocarbons (PAHs) in lake sediments record historic fire events:
829 Validation using HPLC-fluorescence detection. *Org. Geochem.* **45**, 7–17.
830 Diefendorf A. F., Freeman K. H. and Wing S. L. (2014) A comparison of terpenoid and leaf fossil
831 vegetation proxies in Paleocene and Eocene Bighorn Basin sediments. *Org. Geochem.* **71**,
832 30–42.
833 Diefendorf A. F. and Freimuth E. J. (2017) Extracting the most from terrestrial plant-derived n-
834 alkyl lipids and their carbon isotopes from the sedimentary record: A review. *Org.*
835 *Geochem.* **103**, 1–21.
836 Diefendorf A. F., Leslie A. B. and Wing S. L. (2019) A phylogenetic analysis of conifer
837 diterpenoids and their carbon isotopes for chemotaxonomic applications. *Org. Geochem.*
838 **127**, 50–58.
839 Diefendorf A. F., Mueller K. E., Wing S. L., Koch P. L. and Freeman K. H. (2010) Global
840 patterns in leaf 13C discrimination and implications for studies of past and future climate.

Proc. Natl. Acad. Sci. **107**, 5738–5743.
Doerr S. H., Santín C., Merino A., Belcher C. M. and Baxter G. (2018) Fire as a Removal Mechanism of Pyrogenic Carbon From the Environment: Effects of Fire and Pyrogenic Carbon Characteristics. *Front. Earth Sci.* **6**, 1–13.
Dong C. Di, Chen C. F. and Chen C. W. (2012) Determination of polycyclic aromatic hydrocarbons in industrial harbor sediments by GC-MS. *Int. J. Environ. Res. Public Health* **9**, 2175–2188.
Duffin K. I., Gillson L. and Willis K. J. (2008) Testing the sensitivity of charcoal as an indicator of fire events in savanna environments: Quantitative predictions of fire proximity, area and intensity. *Holocene* **18**, 279–291.
Farquhar G. D., Ehleringer J. R. and Hubick K. T. (1989) Carbon Isotope Discrimination and Photosynthesis. *Annu. Rev. Plant Physiol. Plant Mol. Biol.* **40**, 503–537.
Ferrare R. A., Kaufman Y. J. and Fraser R. S. (1990) Satellite measurements of large-scale air pollution: Measurements of forest fire smoke. *J. Geophys. Res.* **95**, 9895–9909.
Freeman K. and Pancost R. D. (2014) Biomarkers for Terrestrial Plants and Climate. *Treatise on Geochemistry*, 395–416.
González-Gaya B., Martínez-Varela A., Vila-Costa M., Casal P., Cerro-Gálvez E., Berrojalbiz N., Lundin D., Vidal M., Mompeán C., Bode A., Jiménez B. and Dachs J. (2019) Biodegradation as an important sink of aromatic hydrocarbons in the oceans. *Nat. Geosci.* **12**, 119–125.
Graham H. V., Patzkowsky M. E., Wing S. L., Parker G. G., Fogel M. L. and Freeman K. H. (2014) Isotopic characteristics of canopies in simulated leaf assemblages. *Geochim. Cosmochim. Acta.*
Grice K., Audino M., Boreham C. J., Alexander R. and Kagi R. I. (2001) Distributions and stable carbon isotopic compositions of biomarkers in torbanites from different palaeogeographical locations. *Org. Geochem.* **32**, 1195–1210.
Grice K., Lu H., Atahan P., Asif M., Hallmann C., Greenwood P., Maslen E., Tulipani S., Williford K. and Dodson J. (2009) New insights into the origin of perylene in geological samples. *Geochim. Cosmochim. Acta* **73**, 6531–6543.
Guillon A., Le Ménach K., Flaud P. M., Marchand N., Budzinski H. and Villenave E. (2013) Chemical characterization and stable carbon isotopic composition of particulate Polycyclic Aromatic Hydrocarbons issued from combustion of 10 Mediterranean woods. *Atmos. Chem. Phys.* **13**, 2703–2719.
Halsall C. J., Sweetman A. J., Barrie L. A. and Jones K. C. (2001) Modelling the behaviour of PAHs during atmospheric transport from the UK to the Arctic. *Atmos. Environ.* **35**, 255–267.
Han Y. M., Bandowe B. A. M., Wei C., Cao J. J., Wilcke W., Wang G. H., Ni H. Y., Jin Z. D., An Z. S. and Yan B. Z. (2015) Stronger association of polycyclic aromatic hydrocarbons with soot than with char in soils and sediments. *Chemosphere* **119**, 1335–1345.
Hanke U. M., Eglinton T. I., Braun A. L. L., Reddy C. M., Wiedemeier D. B. and Schmidt M. W. I. (2016) Decoupled sedimentary records of combustion: Causes and implications. , 5098–5108.
Hanke U. M., Reddy C. M., Braun A. L. L., Coppola A. I., Haghipour N., McIntrye C. P., Wacker L., Xu L., McNichol A. P., Abiven S., Schmidt M. W. I. and Eglinton T. I. (2017) What on Earth Have We Been Burning? Deciphering Sedimentary Records of Pyrogenic Carbon. *Environ. Sci. Technol.* **51**, 12972–12980.
Harper A. R., Santin C., Doerr S. H., Froyd C. A., Albini D., Otero X. L., Viñas L. and Pérez-Fernández B. (2019) Chemical composition of wildfire ash produced in contrasting ecosystems and its toxicity to Daphnia magna. *Int. J. Wildl. Fire* **28**, 726–737.

890 Hilscher A. and Knicker H. (2011) Degradation of grass-derived pyrogenic organic material,
891 transport of the residues within a soil column and distribution in soil organic matter
892 fractions during a 28month microcosm experiment. *Org. Geochem.* **42**, 42–54.
893 Hollander M. and Wolfe D. (1973) *Nonparametric Statistical Methods*., John Wiley & Sons, New
894 York.
895 Holman A. I. and Grice K. (2018) δ 13 C of aromatic compounds in sediments, oils and
896 atmospheric emissions: A review. *Org. Geochem.* **123**, 27–37.
897 Hudspith V. A. and Belcher C. M. (2017) Observations of the structural changes that occur
898 during charcoalification: implications for identifying charcoal in the fossil record.
899 *Palaeontology* **60**, 503–510.
900 Iinuma Y., Brüggemann E., Gnauk T., Müller K., Andreae M. O., Helas G., Parmar R. and
901 Herrmann H. (2007) Source characterization of biomass burning particles: The combustion
902 of selected European conifers, African hardwood, savanna grass, and German and
903 Indonesian peat. *J. Geophys. Res. Atmos.* **112**.
904 Jenkins B. M., Jones A. D., Turn S. Q. and Williams R. B. (1996) Particle concentrations, gas-
905 particle partitioning, and species intercorrelations for polycyclic aromatic hydrocarbons
906 (PAH) emitted during biomass burning. *Atmos. Environ.* **30**, 3825–3835.
907 Kang H. J., Lee S. Y. and Kwon J. H. (2016) Physico-chemical properties and toxicity of
908 alkylated polycyclic aromatic hydrocarbons. *J. Hazard. Mater.* **312**, 200–207.
909 Kappenberg A., Braun M., Amelung W. and Lehndorff E. (2019) Fire condensates and charcoals:
910 Chemical composition and fuel source identification. *Org. Geochem.* **130**, 43–50.
911 Karp A. T., Behrensmeyer A. K. and Freeman K. H. (2018) Grassland fire ecology has roots in
912 the late Miocene. *PNAS* **115**, 12130–12135.
913 Keiluweit M., Kleber M., Sparrow M. A., Simoneit B. R. T. and Prahl F. G. (2012) Solvent-
914 Extractable Polycyclic Aromatic Hydrocarbons in Biochar: In fl uence of Pyrolysis
915 Temperature and Feedstock. *Environ. Sci. Technol.* **46**, 9333–9341.
916 Keiluweit M., Nico P. S. and Johnson M. G. (2010) Dynamic Molecular Structure of Plant
917 Biomass-derived Black Carbon (Biochar). *Environ. Sci. Technol.* **44**, 1–19.
918 Kirchgeorg T., Schüpbach S., Kehrwald N., McWethy D. B. and Barbante C. (2014) Method for
919 the determination of specific molecular markers of biomass burning in lake sediments. *Org.*
920 *Geochem.* **71**, 1–6.
921 Kruskal J. B. (1964) Multidimensional scale by optimizing goodness of fit to a nonmetric
922 hypothesis. *Psychometrika* **29**, 1–27.
923 Laflamme R. E. and Hites R. A. (1978) The global distribution of polycyclic aromatic
924 hydrocarbons in recent sediments. *Geochim. Cosmochim. Acta* **42**, 289–303.
925 Leavitt S. W. and Newberry T. (1992) Systematics of stable-carbon isotopic differences between
926 gymnosperm and angiosperm trees. *Plant Physiol.* **11**, 257–262.
927 Levene H. (1960) Robust Tests for Equality of Variances. In *Contributions to Probability and*
928 *Statistics* (ed. I. Olkin). Stanford University Press, Stanford. pp. 278–292.
929 Leys B. A., Commerford J. L. and McLauchlan K. K. (2017) Reconstructing grassland fire
930 history using sedimentary charcoal: Considering count, size and shape. *PLoS One*.
931 Lima A. L. C., Farrington J. W. and Reddy C. M. (2005) Combustion-Derived Polycyclic
932 Aromatic Hydrocarbons in the Environment—A Review. *Environ. Forensics* **6**, 109–131.
933 Lu H., Zhu L. and Zhu N. (2009) Polycyclic aromatic hydrocarbon emission from straw burning
934 and the influence of combustion parameters. *Atmos. Environ.* **43**, 978–983.
935 Ma Y., Xie Z., Yang H., Möller A., Halsall C., Cai M., Sturm R. and Ebinghaus R. (2013)
936 Deposition of polycyclic aromatic hydrocarbons in the North Pacific and the Arctic. *J.*
937 *Geophys. Res. Atmos.* **118**, 5822–5829.
938 Mackay D. (1998) Partitioning and Physical Chemical Properties of PAHs. In *PAHs and Related*

Compounds (ed. A. N. Neilson). Springer-Verlag.
Mallick S., Chakraborty J. and Dutta T. K. (2011) Role of oxygenases in guiding diverse metabolic pathways in the bacterial degradation of low-molecular-weight polycyclic aromatic hydrocarbons: A review. *Crit. Rev. Microbiol.* **37**, 64–90.
Marynowski L. and Simoneit B. R. T. (2009) Widespread Upper Triassic To Lower Jurassic Wildfire Records From Poland: Evidence From Charcoal and Pyrolytic Polycyclic Aromatic Hydrocarbons. *Palaios* **24**, 785–798.
Masiello C. A. (2004) New directions in black carbon organic geochemistry. *Mar. Chem.* **92**, 201–213.
Maslen E., Grice K., Métayer P. Le, Dawson D. and Edwards D. (2011) Stable carbon isotopic compositions of individual aromatic hydrocarbons as source and age indicators in oils from western Australian basins. *Org. Geochem.* **42**, 387–398.
McBeath A. V., Smernik R. J., Schneider M. P. W., Schmidt M. W. I. and Plant E. L. (2011) Determination of the aromaticity and the degree of aromatic condensation of a thermosequence of wood charcoal using NMR. *Org. Geochem.* **42**, 1194–1202.
McCune B. and Grace J. B. (2002) *Analysis of Ecological Communities Communities*.,
McGrath T. E., Chan W. G. and Hajajigol R. (2003) Low temperature mechanism for the formation of polycyclic aromatic hydrocarbons from the pyrolysis of cellulose. Journal of Analytical and Applied Pyrolysis, v. 66, p. 51-70, 2003. *J. Anal. Appl. Pyrolysis* **66**, 51–70.
Miller D. R., Castañeda I. S., Bradley R. S. and MacDonald D. (2017) Local and regional wildfire activity in central Maine (USA) during the past 900 years. *J. Paleolimnol.* **58**, 455–466.
Nabbefeld B., Grice K., Summons R. E., Hays L. E. and Cao C. (2010) Significance of polycyclic aromatic hydrocarbons (PAHs) in Permian/Triassic boundary sections. *Appl. Geochemistry* **25**, 1374–1382.
Nakamura H. (2019) Plant-derived triterpenoid biomarkers and their applications in paleoenvironmental reconstructions: chemotaxonomy, geological alteration, and vegetation reconstruction. *Results Org. Geochemistry* **35**, 11–35.
Nam J. J., Sweetman A. J. and Jones K. C. (2009) Polynuclear aromatic hydrocarbons (PAHs) in global background soils. *J. Environ. Monit.* **11**, 45–48.
Nam J. J., Thomas G. O., Jaward F. M., Steinnes E., Gustafsson O. and Jones K. C. (2008) PAHs in background soils from Western Europe: Influence of atmospheric deposition and soil organic matter. *Chemosphere* **70**, 1596–1602.
O' Malley V. P. and Burke R. A. (1997) Using GC ± MS / Combustion / IRMS to determine the 13 C / 12 C ratios of individual hydrocarbons produced from the combustion of biomass materialsÐapplication to biomass burning. *Org. Geochem.* **27**, 567–581.
O'Malley V. P., Abrajano T. A. and Hellou J. (1994) Determination of the 13C/12C ratios of individual PAH from environmental samples: can PAH sources be appotioned? *Org. Geochem.* **21**, 809–822.
Oksanen J., Blanchet F. G., Kindt R., Legendre P., Minchin P. R., O'Hara R. B., Simpson G. L., Solymos P., Stevens M. H. H. and Wagner H. (2018) Vegan.
Olivella M. A., Ribalta T. G., De Febrer A. R., Mollet J. M. and De Las Heras F. X. C. (2006) Distribution of polycyclic aromatic hydrocarbons in riverine waters after Mediterranean forest fires. *Sci. Total Environ.* **355**, 156–166.
Oros D. R., Abas M. R. bin, Omar N. Y. M. J., Rahman N. A. and Simoneit B. R. T. (2006) Identification and emission factors of molecular tracers in organic aerosols from biomass burning: Part 3. Grasses. *Appl. Geochemistry* **21**, 919–940.
Oros D. R. and Simoneit B. R. T. (2001a) Identication and emission factors of molecular tracers in organic aerosols from biomass burning Part 1. Temperate climate conifers. *Appl. Geochemistry* **16**, 1513–1544.

988 Oros D. R. and Simoneit B. R. T. (2001b) Identication and emission factors of molecular tracers
989 in organic aerosols from biomass burning Part 2 . Deciduous trees. *Appl. Geochemistry* **16**,
990 1545–1565.
991 Peters M. E. and Higuera P. E. (2007) Quantifying the source area of macroscopic charcoal with a
992 particle dispersal model. *Quat. Res.* **67**, 304–310.
993 Ribeiro S. C., Soares C. P. B., Fehrmann L., Jacovine L. A. G. and von Gadow e K. (2015)
994 Aboveground and belowground biomass and carbon estimates for clonal eucalyptus trees in
995 southeast brazil. *Resvista Árvore* **39**, 353–363.
996 Richter H. and Howard J. . (2000) Formation of polycyclic aromatic hydrocarbons and their
997 growth to soot - a review of chemical reaction pathways. *Prog. Energy Combust. Sci.* **26**,
998 565–608.
999 Rocha A. C. and Palma C. (2019) Source identification of polycyclic aromatic hydrocarbons in
1000 soil sediments: Application of different methods. *Sci. Total Environ.* **652**, 1077–1089.
1001 Saiz G., Wynn J. G., Wurster C. M., Goodrick I., Nelson P. N. and Bird M. I. (2015) Pyrogenic
1002 carbon from tropical savanna burning : production and stable isotope composition.
1003 *Biogeosciences*, 1849–1863.
1004 Santín C., Doerr S. H., Kane E. S., Masiello C. A., Ohlson M., de la Rosa J. M., Preston C. M.
1005 and Dittmar T. (2016) Towards a global assessment of pyrogenic carbon from vegetation
1006 fires. *Glob. Chang. Biol.* **22**, 76–91.
1007 Santín C., Doerr S. H., Merino A., Bucheli T. D., Bryant R., Ascough P., Gao X. and Masiello C.
1008 A. (2017) Carbon sequestration potential and physicochemical properties differ between
1009 wildfire charcoals and slow-pyrolysis biochars. *Sci. Rep.* **7**, 1–11.
1010 Schneider M. P. W., Pyle L. A., Clark K. L., Hockaday W. C., Masiello C. A. and Schmidt M. W.
1011 I. (2013) Toward a "molecular thermometer" to estimate the charring temperature of
1012 wildland charcoals derived from different biomass sources. *Environ. Sci. Technol.* **47**,
1013 11490–11495.
1014 Schulze E.-D., Turner N. C., Nicolle D. and Schumacher J. (2006) Leaf and wood carbon isotope
1015 ratios, specific leaf areas and wood growth of Eucalyptus species across a rainfall gradient
1016 in Australia. *Tree Physiol.* **26**, 479–92.
1017 Scott A. . (2000) The Pre-Quaternary history of fire. *Palaeogeogr. Palaeoclimatol. Palaeoecol.*
1018 **164**, 281–329.
1019 Shen G., Wang W., Yang Y., Ding J., Xue M., Min Y., Zhu C., Shen H., Li W., Wang B., Wang
1020 R., Wang X., Tao S. and Russell A. G. (2011) Emissions of PAHs from indoor crop residue
1021 burning in a typical rural stove: Emission factors, size distributions, and gas-particle
1022 partitioning. *Environ. Sci. Technol.* **45**, 1206–1212.
1023 Shen X., Wan S., Colin C., Tada R., Shi X., Pei W., Tan Y., Jiang X. and Li A. (2018) Increased
1024 seasonality and aridity drove the C4 plant expansion in Central Asia since the Miocene–
1025 Pliocene boundary. *Earth Planet. Sci. Lett.* **502**, 74–83.
1026 Sicard M., Granados-Muñoz M. J., Alados-Arboledas L., Barragán R., Bedoya-Velásquez A. E.,
1027 Benavent-Oltra J. A., Bortoli D., Comerón A., Córdoba-Jabonero C., Costa M. J., del Águila
1028 A., Fernández A. J., Guerrero-Rascado J. L., Jorba O., Molero F., Muñoz-Porcar C., Ortiz-
1029 Amezcua P., Papagiannopoulos N., Potes M., Pujadas M., Rocadenbosch F., Rodríguez-
1030 Gómez A., Román R., Salgado R., Salgueiro V., Sola Y. and Yela M. (2019) Ground/space,
1031 passive/active remote sensing observations coupled with particle dispersion modelling to
1032 understand the inter-continental transport of wildfire smoke plumes. *Remote Sens. Environ.*
1033 **232**, 111294.
1034 Simoneit B. R. T. (1998) Biomarker PAHs in the Environment. In *The Handbook of*
1035 *Environmental Chemistry Vol. 3 Part I PAHs and Related Compounds* (ed. A. H. Neilson).
1036 Springer-Verlag, Berlin Heidelberg. pp. 175–221.

1037 Simoneit B. R. T. (2002) Biomass burning - A review of organic tracers for smoke from
1038 incomplete combustion. *Appl. Geochemistry* **17**, 129–162.
1039 Simoneit B. R. T. (1977) Diterpenoid compounds and other lipids in deep-sea sediments and their
1040 geochemical significance. *Geochim. Cosmochim. Acta* **41**, 463–476.
1041 Simoneit B. R. T. C. (1986) Cyclic terpenoids of the geosphere. In *Biological Markers in the*
1042 *Sedimentary Record,* pp. 43–99.
1043 Stogiannidis E. and Laane R. (2015) Source Characterization of Polycyclic Aromatic
1044 Hydrocarbons by Using Their Molecular Indices: An Overview of Possibilities. In *Reviews*
1045 *of Environmental Contamination and Toxicology* (ed. D. M. Whitacre). Springer
1046 International Publishing, Cham. pp. 49–133.
1047 Thevenon F., Williamson D., Bard E., Anselmetti F. S., Beaufort L. and Cachier H. (2010)
1048 Combining charcoal and elemental black carbon analysis in sedimentary archives :
1049 Implications for past fi re regimes , the pyrogenic carbon cycle , and the human – climate
1050 interactions. *Glob. Planet. Change* **72**, 381–389.
1051 Tipple B. J. and Pagani M. (2007) The Early Origins of Terrestrial C $_4$ Photosynthesis. *Annu. Rev.*
1052 *Earth Planet. Sci.* **35**, 435–461.
1053 Turekian V. C., Macko S. A., Gilhooly W. P., Ballentine D. C., Swap R. J. and Garstang M.
1054 (1995) Bulk and Compound-Specific isotopic characterization of the products of biomass
1055 burning: Laboratory studies. In *Biomass Burning and Global Change* (ed. J. Levine). MIT
1056 Press, Cambridge, MA.
1057 Turekian V. C., Macko S., Ballentine D., Swap R. J. and Garstang M. (1998) Causes of bulk
1058 carbon and nitrogen isotopic fractionations in the products of vegetation burns: laboratory
1059 studies. *Chem. Geol.*, 181–192.
1060 Umbanhowar C. E. and McGrath M. J. (1998) Experimental production and analysis of
1061 microscopic charcoal from wood, leaves and grasses. *Holocene* **8**, 341–346.
1062 Vachula R. S., Huang Y., Longo W. M., Dee S. G., Daniels W. C. and Russell J. M. (2019)
1063 Evidence of Ice Age humans in eastern Beringia suggests early migration to North America.
1064 *Quat. Sci. Rev.* **205**, 35–44.
1065 Vachula R. S. and Richter N. (2017) Informing sedimentary charcoal-based fire reconstructions
1066 with a kinematic transport model. *The Holocene* **28**, 173–178.
1067 Vicente A., Alves C., Monteiro C., Nunes T., Mirante F., Cerqueira M., Calvo A. and Pio C.
1068 (2012) Organic speciation of aerosols from wildfires in central Portugal during summer
1069 2009. *Atmos. Environ.* **57**, 186–196.
1070 Vicente A., Alves C., Monteiro C., Nunes T., Mirante F., Evtyugina M., Cerqueira M. and Pio C.
1071 (2011) Measurement of trace gases and organic compounds in the smoke plume from a
1072 wildfire in Penedono (central Portugal). *Atmos. Environ.* **45**, 5172–5182.
1073 Vitzthum von Eckstaedt C. D., Grice K., Ioppolo-Armanios M., Kelly D. and Gibberd M. (2012)
1074 Compound specific carbon and hydrogen stable isotope analyses of volatile organic
1075 compounds in various emissions of combustion processes. *Chemosphere* **89**, 1407–13.
1076 Wakeham S. G., Schaffner C. and Giger W. (1980) Polycyclic aromatic hydrocarbons in Recent
1077 lake Compounds derived from biogenic precursors during early diagenesis. *Geochim.*
1078 *Cosmochim. Acta* **44**, 415–429.
1079 Wang Z., Bi X., Sheng G. and Fu J. (2009) Characterization of organic compounds and molecular
1080 tracers from biomass burning smoke in South China I: Broad-leaf trees and shrubs. *Atmos.*
1081 *Environ.* **43**, 3096–3102.
1082 Wang Z., Fingas M., Shu Y. Y., Sigouin L., Landriault M., Lambert P., Turpin R., Campagna P.
1083 and Mullin J. (1999) Quantitative characterization of PAHs in burn residue and soot
1084 samples and differentiation of pyrogenic PAH1 from petrogenic PAHs - The 1994 mobile
1085 burn study. *Environ. Sci. Technol.* **33**, 3100–3109.

1086 Whittaker R. H. and Likens G. E. (1973) Primary Production: The Biosphere and Man. *Hum.*
1087 *Ecol.* **1**, 357–369.
1088 Wiedemeier D. B., Abiven S., Hockaday W. C., Keiluweit M., Kleber M., Masiello C. A.,
1089 McBeath A. V., Nico P. S., Pyle L. A., Schneider M. P. W., Smernik R. J., Wiesenberg G.
1090 L. B. and Schmidt M. W. I. (2015a) Aromaticity and degree of aromatic condensation of
1091 char. *Org. Geochem.* **78**, 135–143.
1092 Wiedemeier D. B., Brodowski S. and Wiesenberg G. L. B. (2015b) Pyrogenic molecular markers:
1093 Linking PAH with BPCA analysis. *Chemosphere* **119**, 432–437.
1094 Wiesenberg G. L. B., Lehndorff E. and Schwark L. (2009) Thermal degradation of rye and maize
1095 straw: Lipid pattern changes as a function of temperature. *Org. Geochem.* **40**, 167–174.
1096 Wolf M., Lehndorff E., Wiesenberg G. L. B., Stockhausen M. and Schwark L. (2013) Towards
1097 reconstruction of past fire regimes from geochemical analysis of charcoal. *Org. Geochem.*
1098 **55**, 11–21.
1099 Wright H. and Bailey A. (1982) *Fire Ecology*., Wiley, New York.
1100 Wu Y., Arapi A., Huang J., Gross B. and Moshary F. (2018) Intra-continental wildfire smoke
1101 transport and impact on local air quality observed by ground-based and satellite remote
1102 sensing in New York City. *Atmos. Environ.* **187**, 266–281.
1103 Yunker M. B., Macdonald R. W., Vingarzan R., Mitchell R. H., Goyette D. and Sylvestre S.
1104 (2002) PAHs in the Fraser River basin: a critical appraisal of PAH ratios as indicators of
1105 PAH source and composition. *Org. Geochem.* **33**, 489–515.
1106

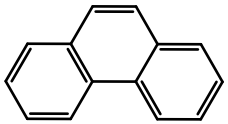

Phenanthrene
(Phen)

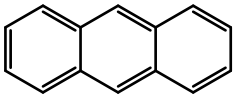

Anthracene
(Ant)

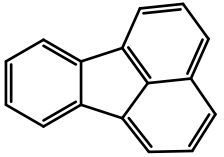

Fluoranthene
(Flu)

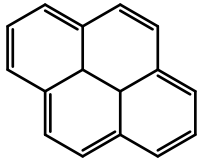

Pyrene
(Pyr)

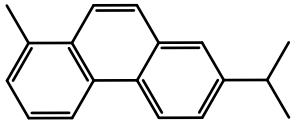

Retene
(Ret)

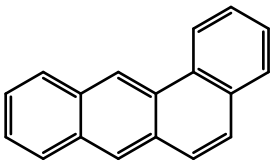

Benz[a]anthracene
(BaA)

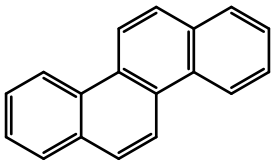

Chrysene
(Chry)

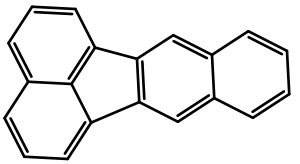

Benzo[f]fluoranthene
(BfF)

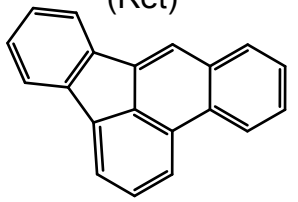

Benzo[b]fluoranthene
(BbF)

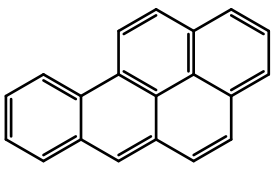

Benzo[a]pyrene
(BaP)

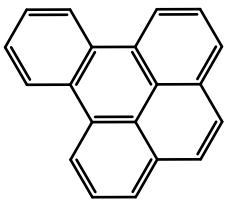

Benzo[e]pyrene
(BeP)

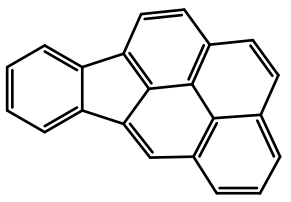

Indeno[1,2,3-cd]pyrene
(IP)

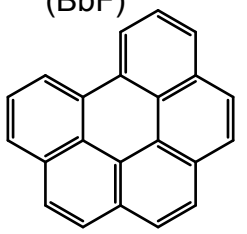

Benzo[ghi]perylene
(BghiP)

	NMDS 1	NMDS 2	r^2	p-value	ρ_{NMDS1}	p-value	ρ_{NMDS2}	p-value
O_2 conditions	-0.99805	-0.06237	0.1988	0.005 **	-0.52	0.001***	-0.04	0.78
Burn Phase	-0.71636	0.69773	0.2307	0.001 ***	-0.48	0.001***	-0.25	0.08*
Plant Functional type	0.09961	-0.99503	0.3693	0.001 ***	0.15	0.28	0.22	0.12
HTT	0.32045	0.94727	0.0798	0.137	0.13	0.37	-0.66	0.001***

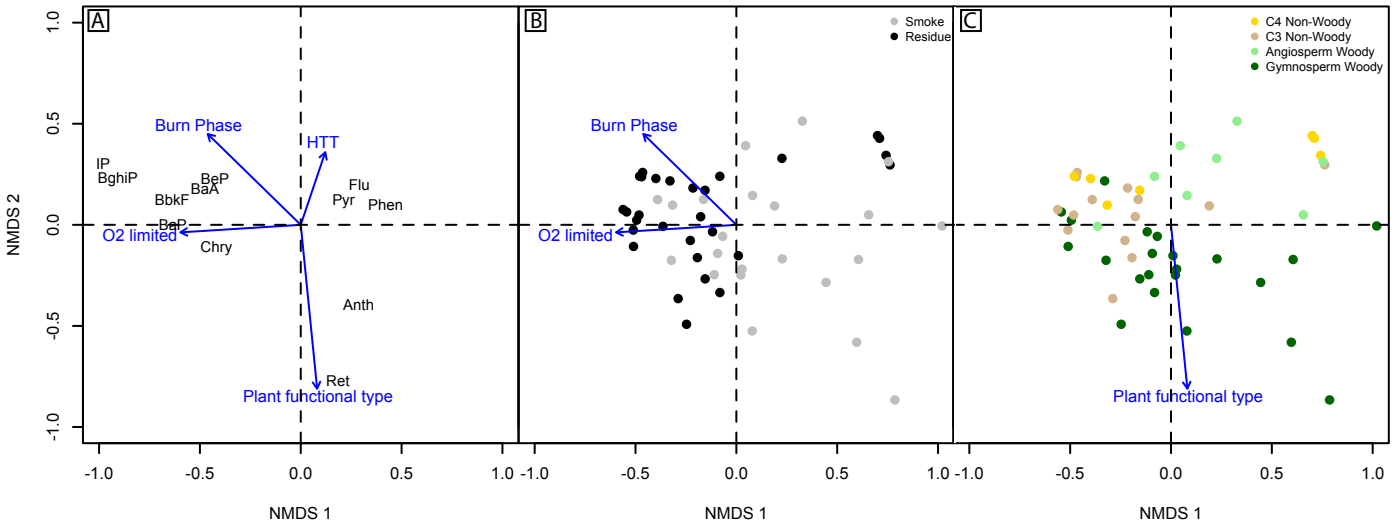

Smoke
Residue
A
Total
D
HTT
E
O_2 Limited
B
Growth Form
C
PFT
ng/g material combusted (log-scale)
ng/g material extracted (log-scale)
5
50
500
5000
300-500°C
<300°C
>600°C
no
yes
W
G
AW
GW
C3G
C4G
NS
***
**

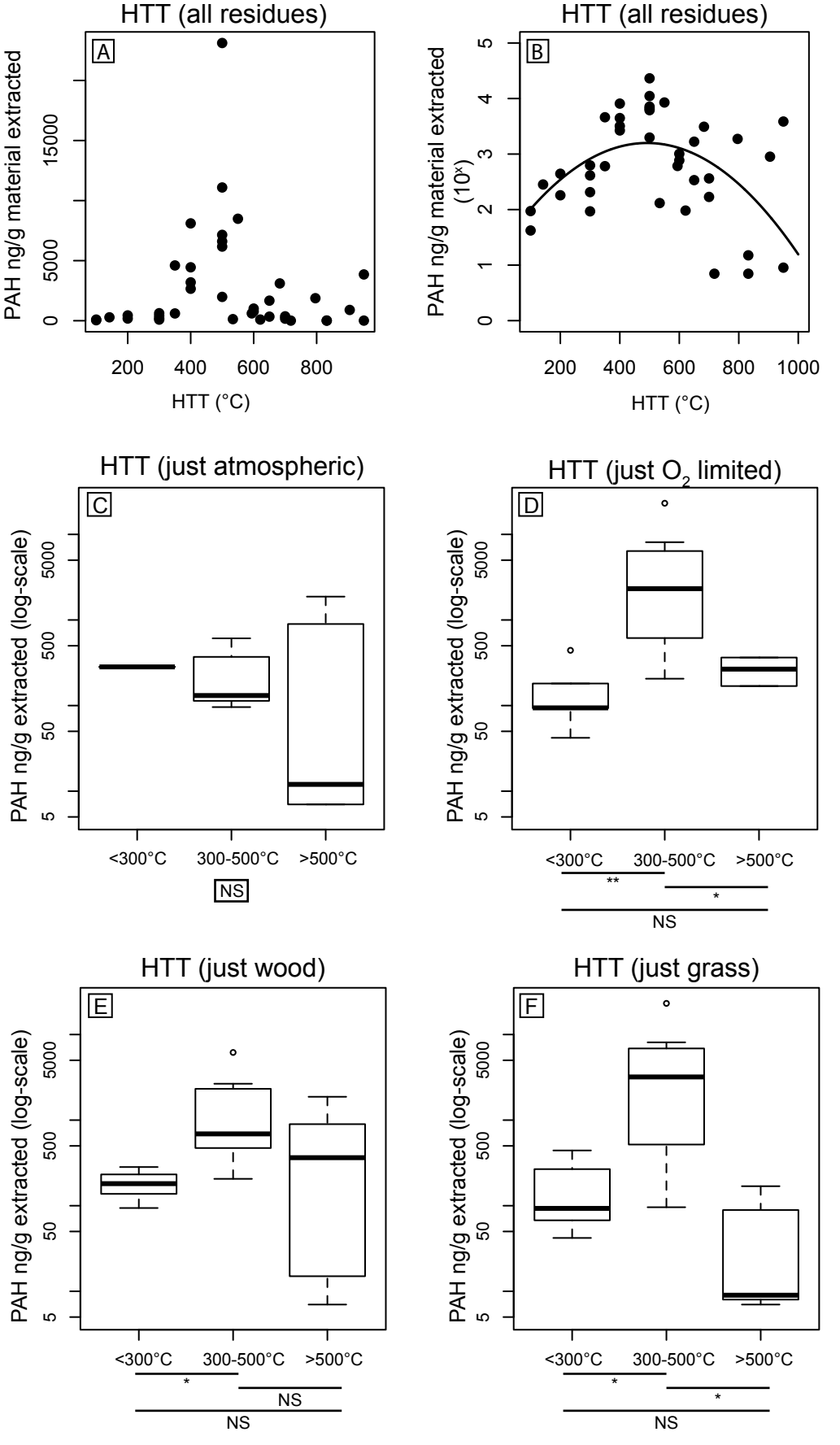
HTT (all residues)
A
PAH ng/g material extracted
0
5000
15000
200
400
600
800
HTT (°C)
HTT (all residues)
B
PAH ng/g material extracted
(10^x)
0
1
2
3
4
5
200
400
600
800
1000
HTT (°C)
HTT (just atmospheric)
C
PAH ng/g extracted (log-scale)
5
50
500
5000
<300°C
300-500°C
>500°C
NS
HTT (just O2 limited)
D
PAH ng/g extracted (log-scale)
5
50
500
5000
<300°C
300-500°C
>500°C
**
*
NS
HTT (just wood)
E
PAH ng/g extracted (log-scale)
5
50
500
5000
<300°C
300-500°C
>500°C
*
NS
NS
HTT (just grass)
F
PAH ng/g extracted (log-scale)
5
50
500
5000
<300°C
300-500°C
>500°C
*
*
NS

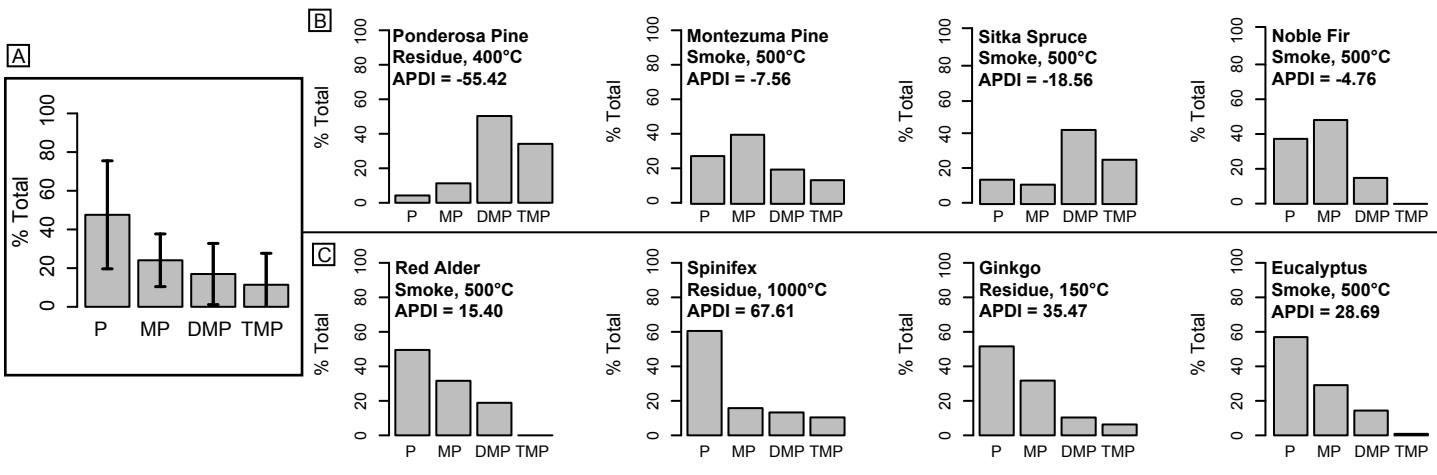
A
% Total
0
20
40
60
80
100
P
MP
DMP
TMP
B
Ponderosa Pine
Residue, 400°C
APDI = -55.42
Montezuma Pine
Smoke, 500°C
APDI = -7.56
Sitka Spruce
Smoke, 500°C
APDI = -18.56
Noble Fir
Smoke, 500°C
APDI = -4.76
C
Red Alder
Smoke, 500°C
APDI = 15.40
Spinifex
Residue, 1000°C
APDI = 67.61
Ginkgo
Residue, 150°C
APDI = 35.47
Eucalyptus
Smoke, 500°C
APDI = 28.69

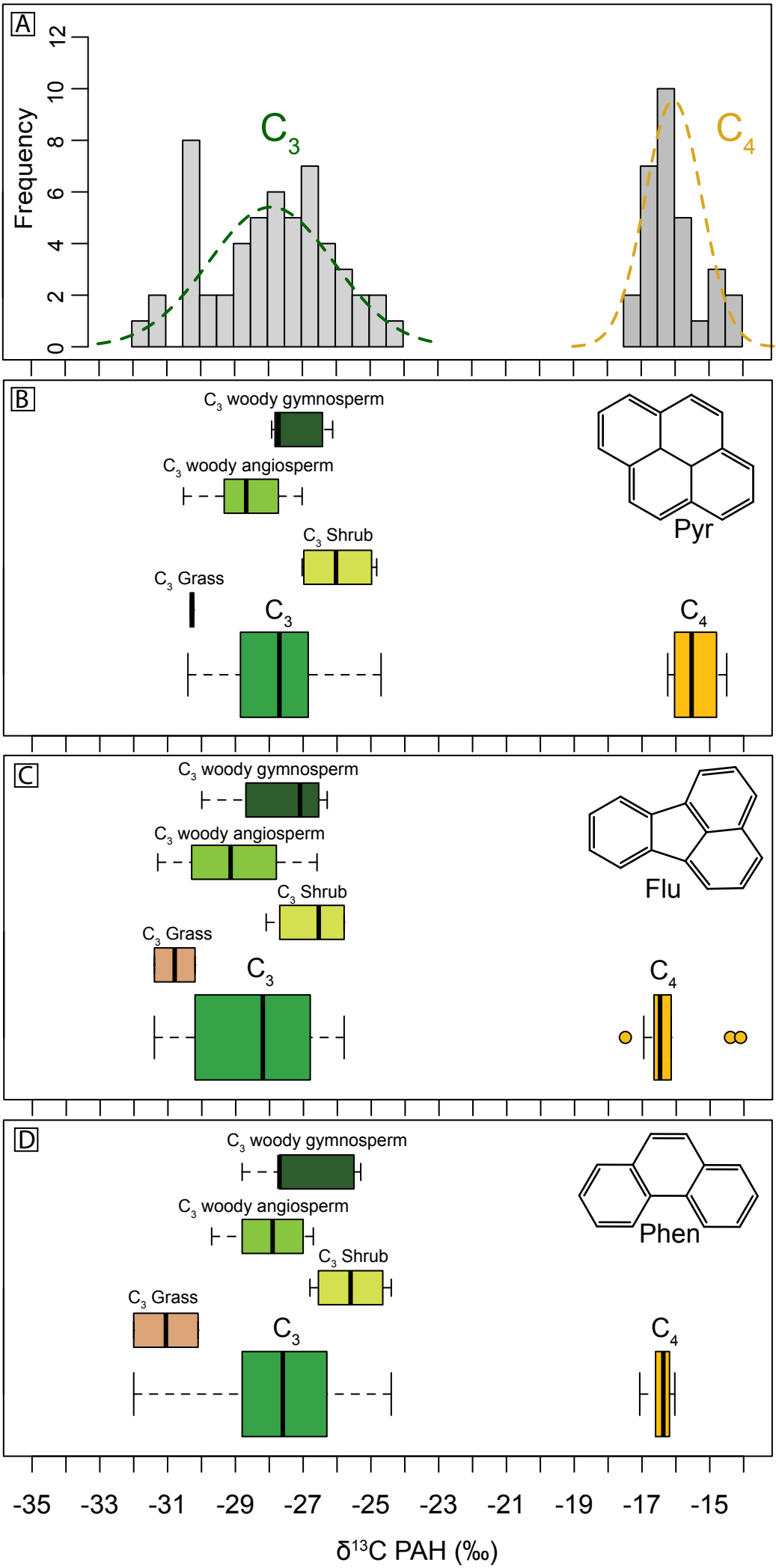
A
Frequency
0
2
4
6
8
10
12
C3
C4
B
C3 woody gymnosperm
C3 woody angiosperm
C3 Shrub
C3 Grass
C3
C4
Pyr
C
C3 woody gymnosperm
C3 woody angiosperm
C3 Shrub
C3 Grass
C3
C4
Flu
D
C3 woody gymnosperm
C3 woody angiosperm
C3 Shrub
C3 Grass
C3
C4
Phen
-35
-33
-31
-29
-27
-25
-23
-21
-19
-17
-15
δ13C PAH (‰)

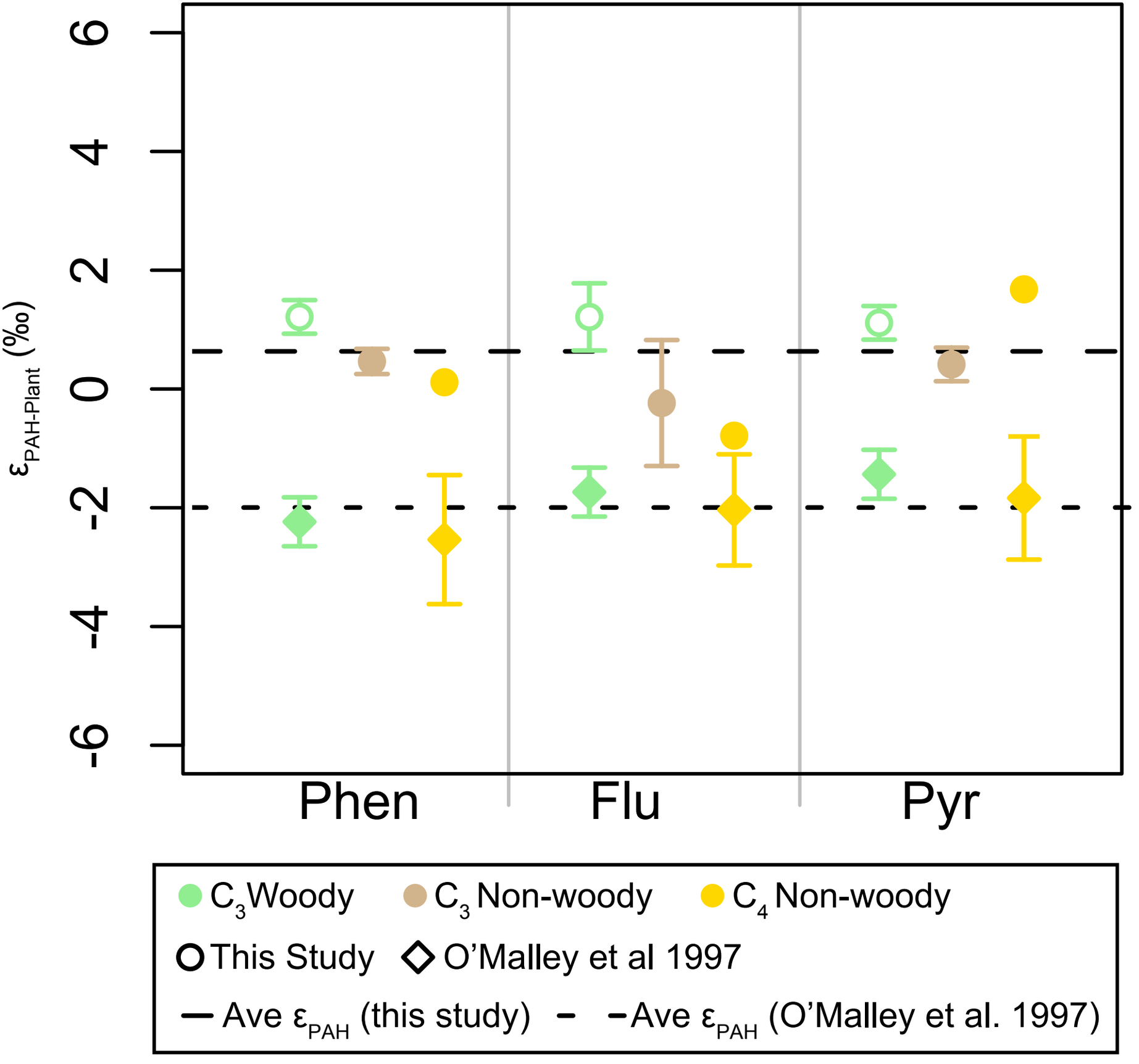
6
4
2
0
-2
-4
-6
$\varepsilon_{PAH\text{-}Plant}$ (‰)
Phen
Flu
Pyr
C_3 Woody
C_3 Non-woody
C_4 Non-woody
This Study
O'Malley et al 1997
Ave ε_{PAH} (this study)
Ave ε_{PAH} (O'Malley et al. 1997)

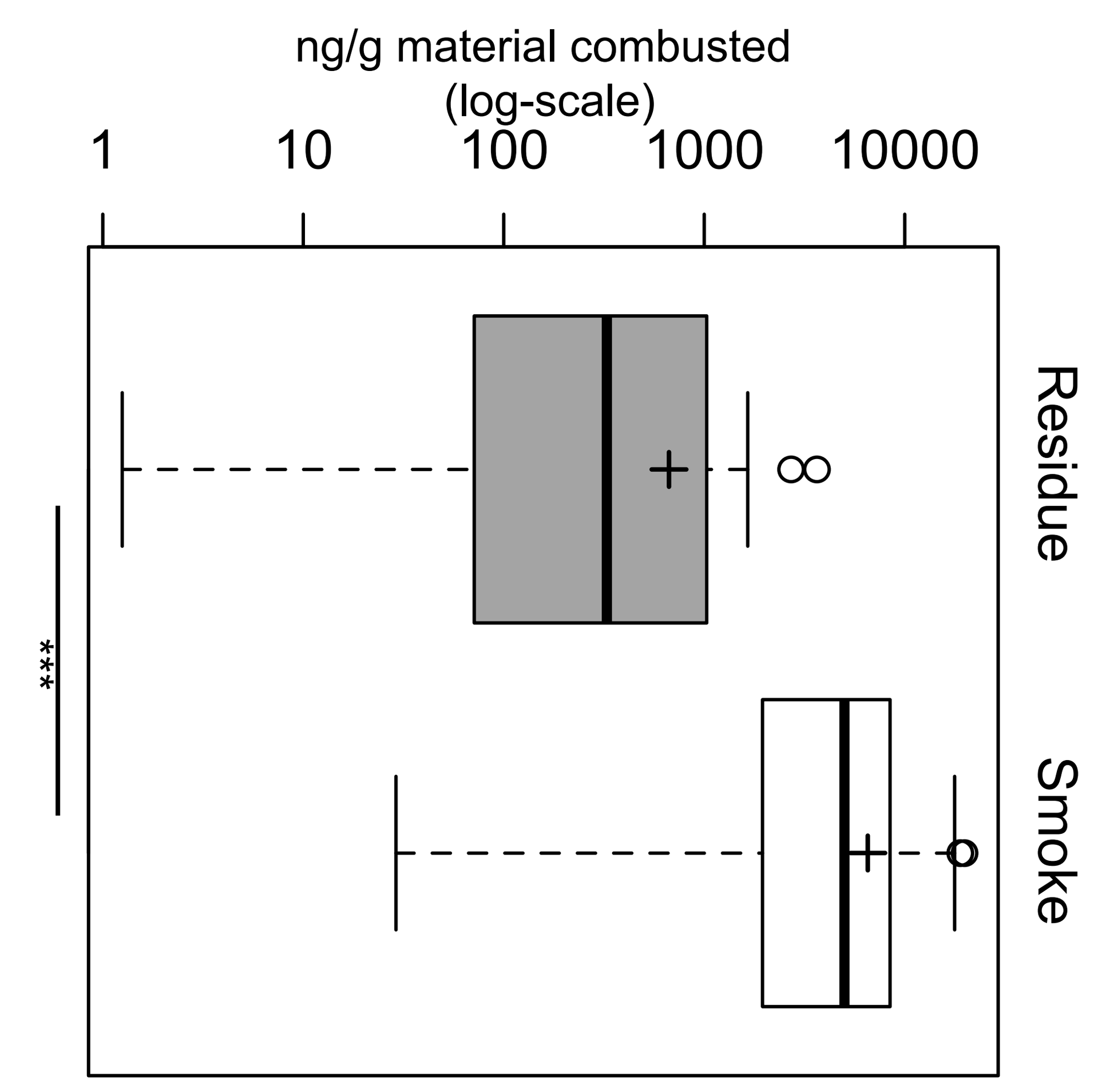
ng/g material combusted
(log-scale)
1
10
100
1000
10000
Residue
8
***
Smoke
9

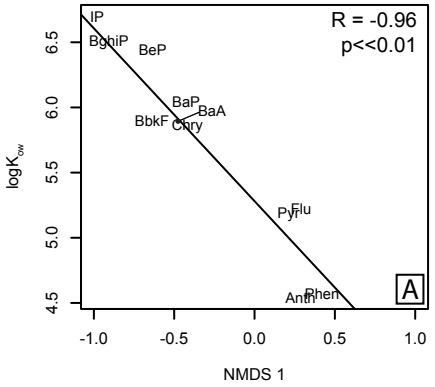
R = -0.96
p<<0.01
IP
BghiP
BeP
BaP
BaA
BbkF
Chry
Pyr
Flu
Anth
Phen
A
logK_ow
NMDS 1

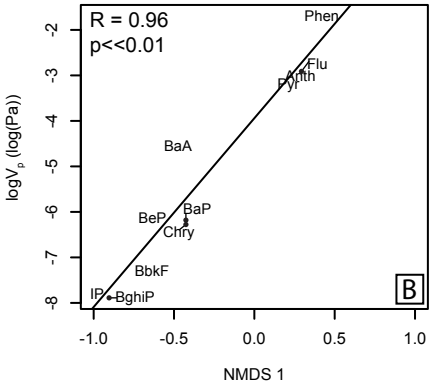
R = 0.96
p<<0.01
Phen
Flu
Anth
Pyr
BaA
BeP
BaP
Chry
BbkF
IP
BghiP
B
logV_p (log(Pa))
NMDS 1

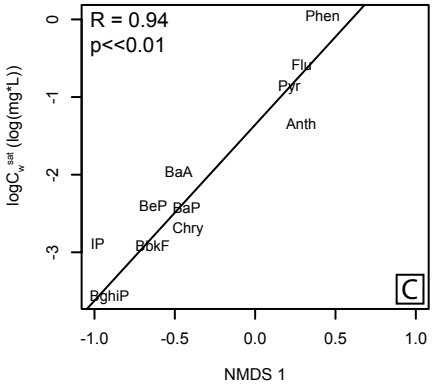
R = 0.94
p<<0.01
Phen
Flu
Pyr
Anth
BaA
BeP
BaP
Chry
IP
BbkF
BghiP
C
logC_w^sat (log(mg*L))
NMDS 1

A
LMW/Total
0.0
0.4
0.8
residue
smoke
B
Ret/(Ret+3-ring)
0.0
0.4
0.8
angio
gymno

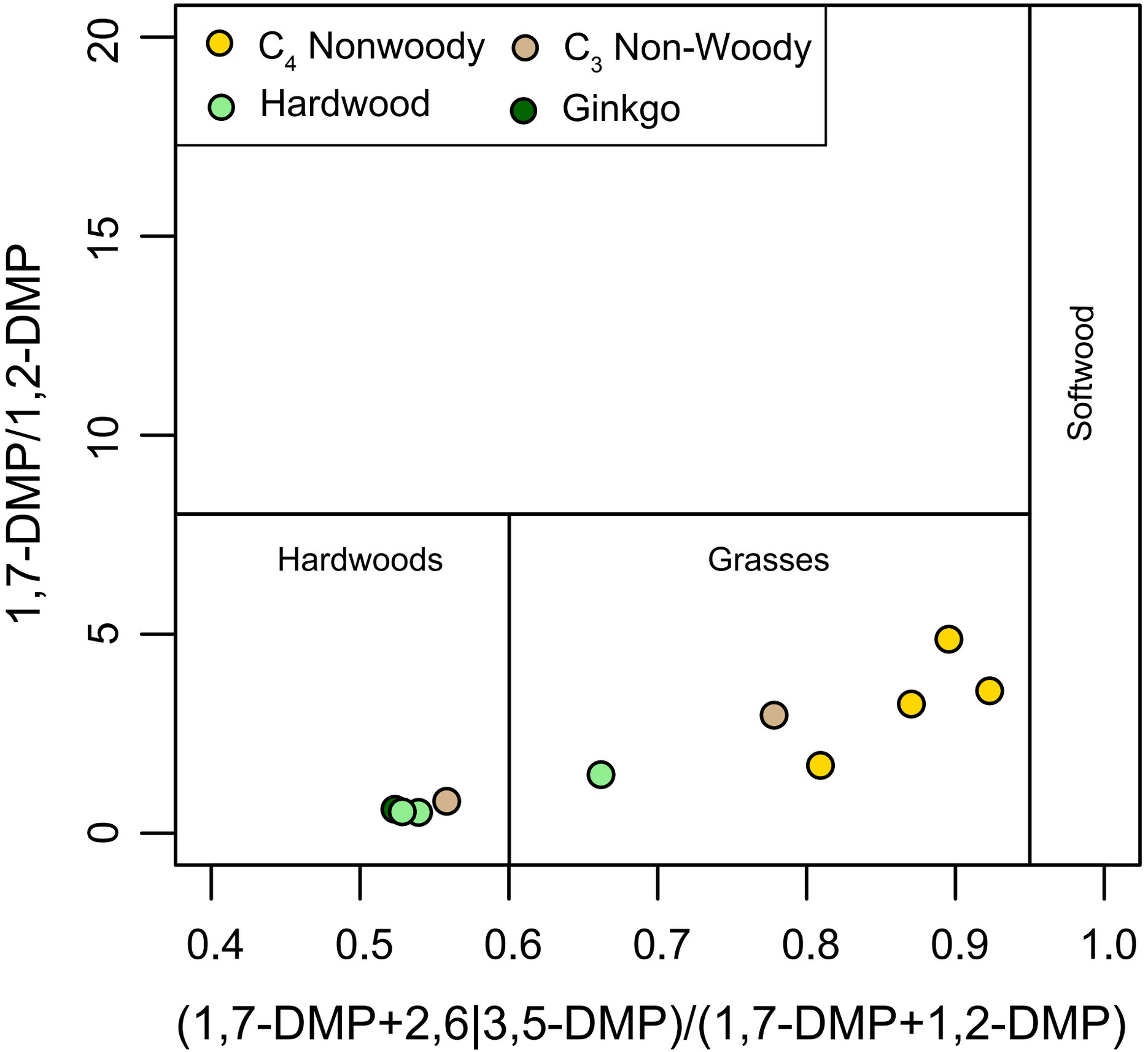
C4 Nonwoody
C3 Non-Woody
Hardwood
Ginkgo
Hardwoods
Grasses
Softwood
1,7-DMP/1,2-DMP
0
5
10
15
20
0.4
0.5
0.6
0.7
0.8
0.9
1.0
(1,7-DMP+2,6|3,5-DMP)/(1,7-DMP+1,2-DMP)

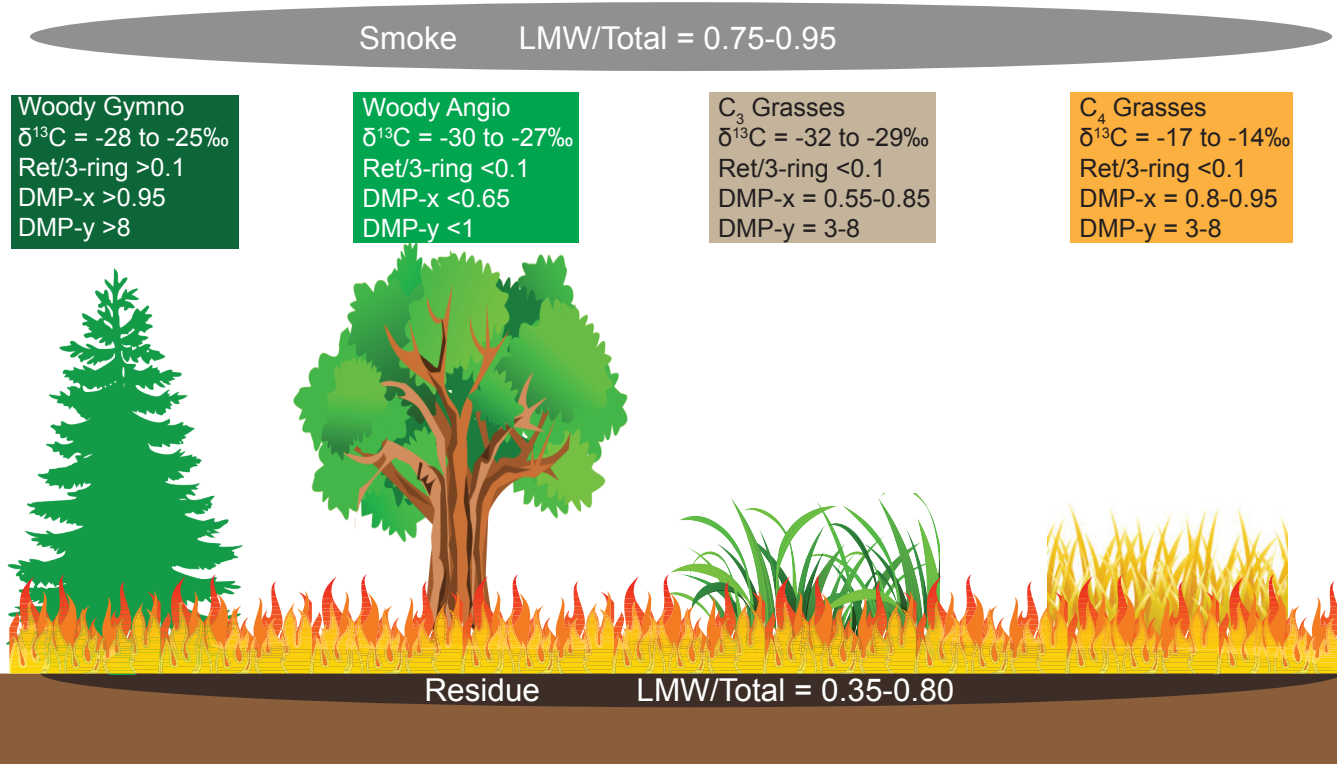
Smoke LMW/Total = 0.75-0.95
Woody Gymno
δ13C = -28 to -25‰
Ret/3-ring >0.1
DMP-x >0.95
DMP-y >8
Woody Angio
δ13C = -30 to -27‰
Ret/3-ring <0.1
DMP-x <0.65
DMP-y <1
C3 Grasses
δ13C = -32 to -29‰
Ret/3-ring <0.1
DMP-x = 0.55-0.85
DMP-y = 3-8
C4 Grasses
δ13C = -17 to -14‰
Ret/3-ring <0.1
DMP-x = 0.8-0.95
DMP-y = 3-8
Residue LMW/Total = 0.35-0.80

Study	Experiment apperatus	Type of data	Burn Phase	O2 conditions	Plant Functional Types	# of samples
Oros & Simoneit 2001a	Open burn	Concentration	Smoke	atmospheric	Woody Gymnosperm	13
Oros & Simoneit 2001b	Open burn	Concentration	Smoke	atmospheric	Woody Angiosperm	5
Oros & Simoneit 2006	Open burn	Concentration	Smoke	atmospheric	C3 and C4 grasses	4
Santín et al 2017	Open burn and muffle furance	Concentration	Residue	both	Woody Gymnosperm	4
Keiluit et al 2012	Muffle furnace	Concentration	Residue	limited	Woody Gymnosperm and C3 grasses	14
Weisenberg et al 2009	Muffle furnace	Concentration	Residue	limited	C3 and C4 grasses	6
O'Malley et al. 1997	Combustion furnace	Isotopes	Smoke	atmospheric	Woody Angiosperm and C4 grasses	8
Gullion et al. 2013	Fireplace	Isotopes	Smoke	atmospheric	Woody Angiosperm, Woody Gymnosperm, and C3 grasses	14
This study	Open burn	Both	Residue	atmospheric	Woody Angiosperm, Woody Gymnosperm, C4 grasses, and C3 grasses	10

Ratio name	Mathematical equation	Presented in this work or previous study	Interpretation	Future work
APDI	For a parabolic curve fit to a normalized alkylated PAH distribution: $f(x) = ax^2 + bx + c$; [f''(x) - f '(2)] = APDI	This work; New descriptive index, but based on insights from Blumer and Youngblood (1975), Laflamme and Hites (1978), and Stogiannidis and Laane (2015)	Differentiating between pyrogenic or petrogenic source of PAHs. Pyrogenic >0 Petrogenic OR conifer <0	Verification through application to sediments with mixed sources
DMP-x	(1,7-DMP+2,6|3,5-DMP)/(1,7-DMP+2,6|3,5-DMP+1,2-DMP)	Kappenberg et al. (2019); based on observations that hardwood combustion products were dominated by 1,2-DMP, softwood products was dominated by 1,7-DMP, and grass products had equal contributions of all of these DMP isomers.	Identifying changes in which plant community burned. Hardwood (>0.95) Softwood (<0.65) Grasses (0.55-0.85)	Measurements in additional plant species and functional groups; Verification through application to sediments
DMP-y	(1,7-DMP)/(1,2-DMP)	Kappenberg et al. (2019); based on observations that hardwood combustion products were dominated by 1,2-DMP, softwood products was dominated by 1,7-DMP, and grass products had equal contributions of all of these DMP isomers.	Identifying changes in which plant community burned. Hardwood (>8) Softwood (<1) Grasses (3-8)	Measurements in additional plant species and functional groups; Verification through application to sediments
LMW/ Total	(Phen+Ant+Flu+Pyr)/(Phen+Ant+Flu+Pyr+BaA+Chry+BkfF+BeP+BaP+IP+BghiP)	This work; Produced from seperations by molecular wieght along NMDS axis 1, which correlated strongly with burn phase. Molecular weight ratios are widely used to examine PAHs but are generally interpreted as changes in source in environmental settings (i.e., petrogenic v. pyrogenic) (e.g., Tobiszewski and Namieśnik, 2012; Wolska et al., 2012; Stogiannidis and Laane, 2015) or fire intensity in geologic records (e.g., Finkelstein et al., 2005; Denis et al., 2012)	Differentiating between PAHs derived from smoke or combustion residues. Residue (0.35-0.8) Smoke (0.75-0.95)	Verification through measurements of smoke and char in natural wildfires and application to sediments
Ret/3-ring	Ret/(Ret+Phen+Ant)	This work; Produced from seperation of retene along NMDS axis 2, which correlated strongly with plant functional type. Retene is widely used to examine conifer inputs (e.g., Simoneit, 1977; Miller et al., 2017), but this ratio are its associated ranges are novel.	Identifying changes in which plant community burned. Gymnosperm (>0.1) Angiosperm (<0.1)	Verification through application to sediments

References Cited: Blumer M. . and Youngblood W. (1975) Polycyclic Aromatic Hydrocarbons in Soils and Recent Sediments. Science (80-.). 188, 53–55.
Denis E. H., Toney J. L., Tarozo R., Scott Anderson R., Roach L. D. and Huang Y. (2012) Polycyclic aromatic hydrocarbons (PAHs) in lake sediments record historic fire events: Validation using HPLC-fluorescence detection. Org. Geochem. 45, 7–17. Available at: http://dx.doi.org/10.1016/j.orggeochem.2012.01.005.
Finkelstein D. B., Pratt L. M., Curtin T. M. and Brassell S. C. (2005) Wildfires and seasonal aridity recorded in Late Cretaceous strata from south-eastern Arizona, USA. Sedimentology 52, 587–599.
Kappenberg A., Braun M., Amelung W. and Lehndorff E. (2019) Fire condensates and charcoals: Chemical composition and fuel source identification. Org. Geochem. 130, 43–50. Available at: https://doi.org/10.1016/j.orggeochem.2019.01.009.
Laflamme R. E. and Hites R. A. (1978) The global distribution of polycyclic aromatic hydrocarbons in recent sediments. Geochim. Cosmochim. Acta 42, 289–303.
Miller D. R., Castañeda I. S., Bradley R. S. and MacDonald D. (2017) Local and regional wildfire activity in central Maine (USA) during the past 900 years. J. Paleolimnol. 58, 455–466.
Simoneit B. R. T. (1977) Diterpenoid compounds and other lipids in deep-sea sediments and their geochemical significance. Geochim. Cosmochim. Acta 41, 463–476.
Stogiannidis E. and Laane R. (2015) Source Characterization of Polycyclic Aromatic Hydrocarbons by Using Their Molecular Indices: An Overview of Possibilities. In Reviews of Environmental Contamination and Toxicology (ed. D. M. Whitacre). Springer International Publishing, Cham. pp. 49–133. Available at: http://dx.doi.org/10.1007/978-3-319-10638-0_2.
Tobiszewski M. and Namieśnik J. (2012) PAH diagnostic ratios for the identification of pollution emission sources. Environ. Pollut. 162, 110–119.
Wolska L., Mechlińska A., Rogowska J. and Namieśnik J. (2012) Sources and fate of PAHs and PCBs in the marine environment. Crit. Rev. Environ. Sci. Technol. 42, 1172–1189.